Icarus 441 (2025) 116673

Contents lists available at ScienceDirect

Icarus

journal homepage: www.elsevier.com/locate/icarus

Research Paper

Geological analysis of the dome field in western Utopia Planitia, on Mars

Javier Eduardo Suárez-Valencia [a,*], Angelo Pio Rossi [b], Monica Pondrelli [c], Lucia Marinangeli [c], Vikram Unnithan [a]

[a] Constructor University, Bremen, Germany
[b] Earthgraph GmbH, Germany
[c] Università degli Studi "G. d'Annunzio" Chieti – Pescara, Italy

ARTICLE INFO

Keywords:
Mars
Planetary geology
Volcanism
Remote sensing

ABSTRACT

Hundreds of domes are scattered over a plain composed of different geological units in the western margin of Utopia Planitia, near the northern martian dichotomy. These structures have traditionally been considered of igneous origin. In this work, we utilized recent data to study the geomorphological and compositional properties of this dome field. We found that the domes originated from an intrusive-to-extrusive system, since they range from cryptodomes to volcanic domes. Each dome appears to represent a single magmatic event, indicating they formed in a monogenetic regime. Two main groups of domes were identified according to their shapes and stratigraphic relationships with the floor units, which represent two different stages of igneous activity. It was established from a linear analysis that the domes are preferentially aligned following a NW-SE trend, which is consistent with the regional faults and fractures. The domes field in Utopia Planitia was likely created by two monogenetic magmatic events at different ages, which took advantage of the tectonic configuration of the area to be emplaced. Some magmas were able to reach the surface creating extrusive structures, while the majority crystalized near the surface creating intrusive ones. Of the last group, the majority were uncovered by tectonic or erosive processes, while a small number of them remained trapped underground as cryptodomes. This sequence of events would explain the large distribution of the domes, as well as the wide variety of morphologies that we observe today.

1. Introduction

Martian landforms of volcanic origin are morphologically and genetically diverse, they are also widely distributed across the surface. Many of them are located near the large volcanoes in the Tharsis region (e.g. Williams et al., 2008; Mouginis-Mark, 2018), where lava flows, dyke swarms, calderas, cones, and several other structures are commonly found (e.g. Bleacher et al., 2007; Hynek et al., 2003; Brož et al., 2021; Hauber et al., 2011; Pieterek et al., 2022). However, intrusive structures, particularly intrusive domes, have only been reported in a few instances (Rampey et al., 2007; Farrand et al., 2011; Michaut et al., 2013).

Intrusive and extrusive domes are often harder to recognize than other igneous landforms, mainly because there are several geological processes on Mars that can result in dome-like structures. For example, fields of knobs, mesas, pingos, mud volcanoes, and mounds are found in the northern martian plains, each with varied, non-igneous origins (e.g. Zhang et al., 2023; Soare et al., 2013; Ivanov et al., 2014; Oehler and Allen, 2010). Therefore, a detailed geomorphological and spectral analysis is needed to differentiate between these structures.

Two locations with potential igneous domes in the northern plains of Mars were identified and studied by Rampey et al. (2007), Farrand et al. (2011), and Farrand et al. (2021). The first one is in Arcadia Planitia (between 34 and 46°N and 167–180°E), this location was extensively studied by both authors. The second location is in Utopia Planitia (between 37 and 46°N and 76–86°E), and it was only partially examined by Farrand et al. (2011). In both cases, hundreds of domes are scattered across a large area, intercepting different geological units. This assemblage is commonly known as a "Dome field".

In this work, we analyzed the dome field in Utopia Planitia with recent data to understand how they formed, and to establish similarities and differences with the better understood dome field on Arcadia Planitia.

* Corresponding author at: Johann Bornemacher 30, 28217 Bremen, Germany.
E-mail address: jsuarezvalencia@constructor.university (J.E. Suárez-Valencia).

https://doi.org/10.1016/j.icarus.2025.116673
Received 7 February 2025; Received in revised form 27 May 2025; Accepted 28 May 2025
Available online 31 May 2025

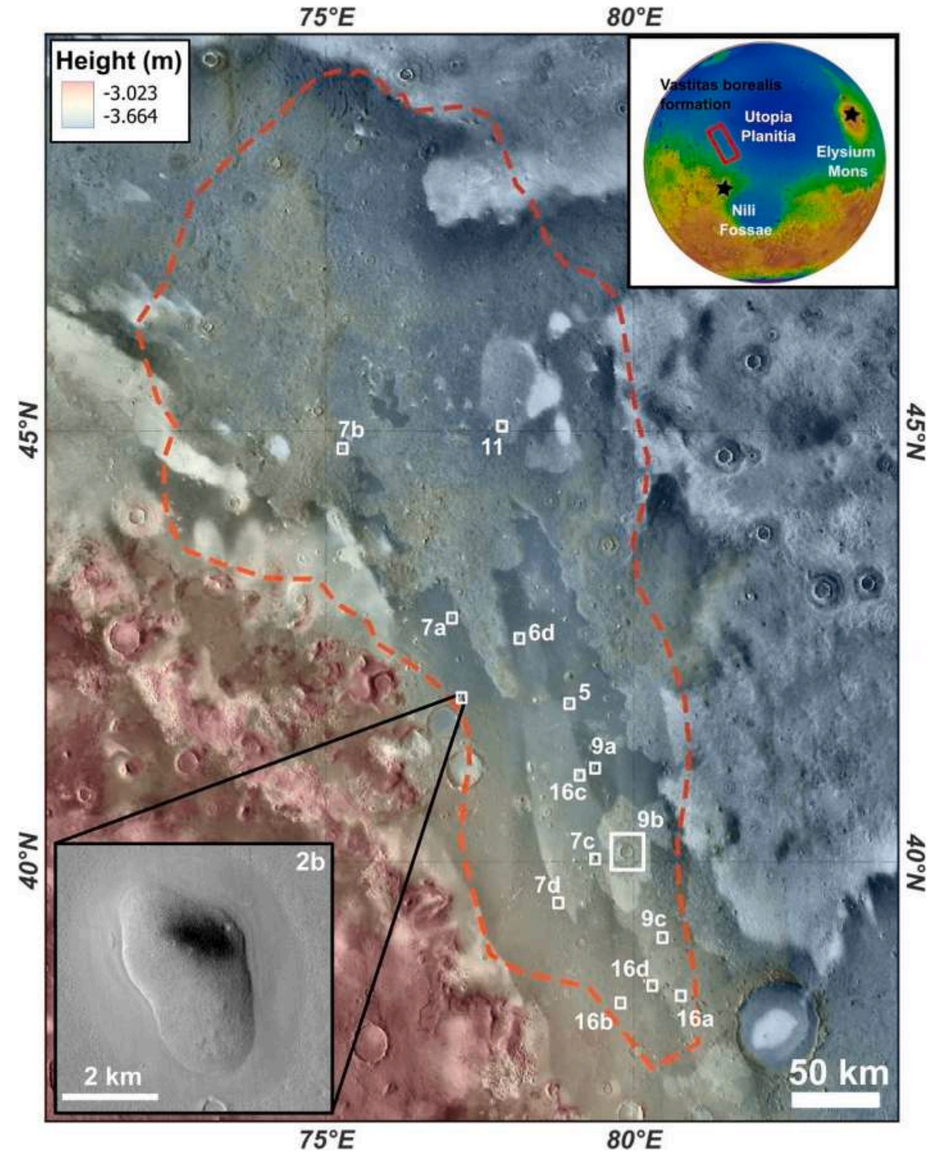

Fig. 1. Location of the dome field on Utopia Planitia. The white boxes indicate the location of the domes showcased in the respective figures. The basemap are the THEMIS day infrared mosaic and the MOLA-HRSC DEM.

2. Geological setting

2.1. Location on Utopia Planitia

Utopia Planitia is one of the largest impact basins on Mars. It is situated in the northern plains of the planet, west of Elysium Mons and north of Nili Fossae (Fig. 1). Ice-related and periglacial activity are thought to be important agents in the geologic evolution of the area, since thick ice-dust mantles and periglacial landforms are present across the basin (Soare et al., 2012).

The dome field in Utopia Planitia lies along the western margin of the basin (between 37–46°N and 76–86°E). To the southeast are Nilosyrtis Mensae, a fretted terrain thought to be formed by groundwater runoff (Bandfield and Amador, 2016), while to the northeast lies the extensive Vastitas Borealis formation, a flat deposit of mixed sediments whose origin is unclear but thought to be related to a hypothesized ancient ocean, outflow channels deposits or subsurface water sources (Liu et al., 2022). Most of the domes occur in a broad, nearly flat terrain, which gently slopes towards the northeast, to the center of the basin. The concentration of domes decreases gradually towards the east and south, where other dome-like structures such as mesas or pingos also appear (Mills et al., 2021). To narrow our research, we defined a study area of 141,000 km^2, focused on the regions with the highest concentration of candidate igneous domes (Fig. 1).

The study area was previously mapped by Tanaka et al. (2005). Due to mapping scale constraints, the domes themselves were not specifically noted, but their location in the map would correspond to a transitional area between the highlands and the northern lowlands. Most of the domes are located in the Utopia Planitia 2 unit ($\boldsymbol{HBu_2}$), which according to the authors is made of eroded remains of a Hesperian basement. Other domes are found in the Vastitas Borealis Marginal formation ($\boldsymbol{ABv_m}$), which is believed to be made of deposits associated with outflow events. More domes lie over the Astapus Colles unit (***ABa***), which is thought to be a volatile-rich mantle made of debris mobilized from the prior units, and that later was heavily degraded by the action of ice and wind.

2.2. The dome field in Arcadia Planitia

The properties of the domes in Arcadia Planitia are relevant for this research due to their similarities to the ones in Utopia Planitia, as in our area, hundreds of domes are scattered over a vast and open plain. Numerous wrinkle rides cross the area and are spatially related to the

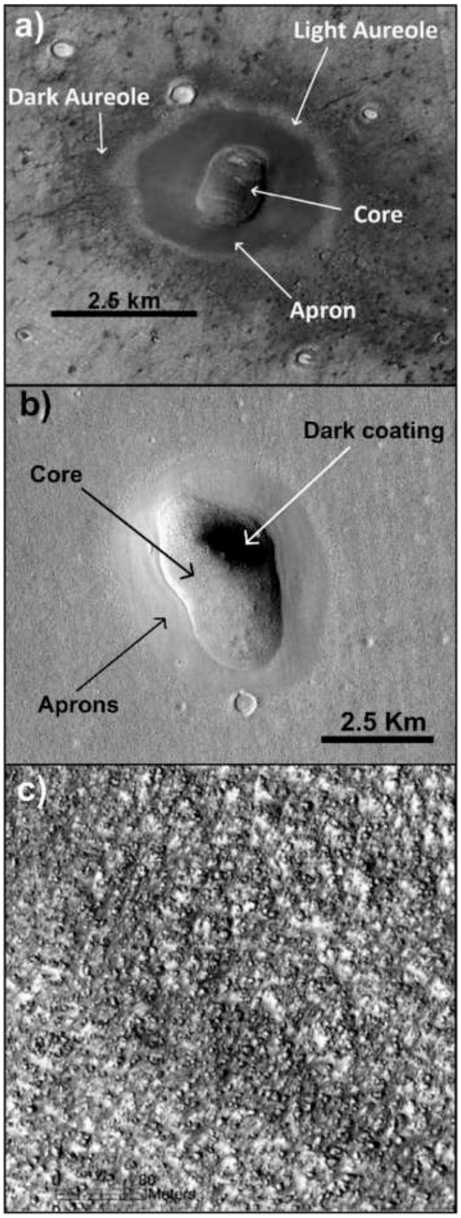

Fig. 2. CTX images showing the structure of the domes. a) Typical structure of the domes in Arcadia Planitia, showing a core, aprons, and aureoles (center coordinates: 39.07°N, 172.41°E) (Taken from Farrand et al., 2021). b) Typical structure of the domes in Utopia Planitia, showing a core, aprons, and a dark coating, but lacking aureole (center coordinates: 41.91°N, 77.19°E). c) Blocky texture on top of the domes in Arcadia Planitia (Taken from Farrand et al., 2011).

domes (Rampey et al., 2007). Each dome consists of a central core, radial aprons accumulated around them, and an aureole of light or dark-toned deposits (Fig. 2) (Farrand et al., 2011). The cores have a high thermal inertia, suggesting they are composed of solid rock, although their surface is covered by unconsolidated blocky materials (Fig. 2c). The aprons are sediments covering the flanks and surroundings of the domes, which would be consistent with debris falling from the cores, either by the action of mass waste or ice-related dynamics (Farrand et al., 2011). Finally, the aureole is distal zones with evidence of periglacial and sublimation textures. Aureole shows the particular “Brain terrain”, a texture thought to be formed by the cracking of ice-rich surfaces due to thermal and glacial stresses (Levy et al., 2009).

Rampey et al. (2007) further classified the domes into two groups. The first type, the “core-annulus-aureole” (CCA) domes, was described above. These domes were interpreted as extrusive in origin, since they are clearly uncovered, and some show lobate structures and pitted summits. The second type, known as “Blister” or cryptodomes, appears as small bumps in the plain, with no aprons or aureole. Furthermore, these cryptodomes appear to be covered by the material that makes up the plains, since they do not have any textural or spectral contrast with their surroundings. This leads Rampey et al. (2007) to classify these structures as intrusive domes that were emplaced near the surface. Farrand et al. (2011) proposed a formation model for both types of domes which involves several steps. First, the domes were emplaced near the surface, creating a fractured carapace rich in hyaloclastite breccia where the intrusions meet the host rock. Second, the domes were exhumated by erosion or tectonics, leading to the formation of the aprons from the hyaloclastite carapace. Finally, all the mobilized material underwent the effect of ice and wind, forming the distal aureole and their characteristic textures.

Farrand et al. (2021) used hyperspectral data to check the composition of the domes. They found strong absorptions at 1 and 2 μm, which would be consistent with a mixture of olivine, pyroxenes and glass (Burns, 1993; Sunshine and Pieters, 1998). Farrand et al. (2021) also detected an anomalous absorption around 1.3 μm which could be linked to the presence of Fe-rich plagioclase, and a particular spectral convexity between 3.4 and 3.9 μm, associated with rocky, light-toned portions on top of some domes, and which is attributed to the presence of alkali feldspars (Brown and Pritchard, 1968). This mineralogy suggests an intermediate-to-felsic composition for the magmas that formed the domes.

Many of the previous descriptions also apply for the domes on Utopia Planitia (Fig. 2b). However, they have some morphological differences compared to the ones on Arcadia Planitia, like the absence of aureoles, the materials covering the domes, and the size of some structures. These differences may be related to the distinct geological settings between the two locations.

3. Data

Since the domes are spread over a large area, we used medium-resolution datasets to analyze the properties of the materials in which the domes were emplaced (here called floor units), and their stratigraphic relationships with the surrounding terrains. This was mainly done using the global mosaic derived from the Context Camera (CTX) onboard the Mars Reconnaissance Orbiter (MRO) (Malin et al., 2007). This panchromatic mosaic covers the area with an average resolution of 5 m/pixel (Dickson et al., 2024). Other global datasets used were the day and night thermal inertia mosaics derived from the Thermal Emission Imaging System (THEMIS) onboard Mars Odyssey, which has a spatial resolution of 100 m/pixel (Edwards et al., 2011), these datasets were used to check if the materials around the domes were rock bodies or unconsolidated sediments. In locations not well-covered by CTX data, multispectral images from the High Resolution Stereo Camera (HRSC) onboard Mars Express were used (Gwinner et al., 2016). To gather terrain information, we used the global Digital Elevation Model (DEM) derived from the Mars Orbital Laser Altimeter (MOLA) and the High Resolution Camera (HRSC) onboard Mars Express, offering a spatial resolution of 200 m/pixel (Fergason et al., 2018). Also, in areas that were covered by CTX stereopairs, we derived DEMs using the MarsSI web service (Quantin-Nataf et al., 2018).

To study the individual domes and other small-scale features on the area we used high resolution datasets retrieved from the Planetary Data System (PDS). First, several panchromatic images captured by the High Resolution Imaging Science Experiment (HiRISE) onboard MRO were used (see Annex 1); these images have an average spatial resolution of 50 cm/pixel (McEwen, 2007). Second, we utilized CRISM hyperspectral cubes to analyze the composition, we downloaded the Map-Projected Targeted Reduced Data Record (MTRDR) version of the cubes. These products have several advantages since they have units in corrected

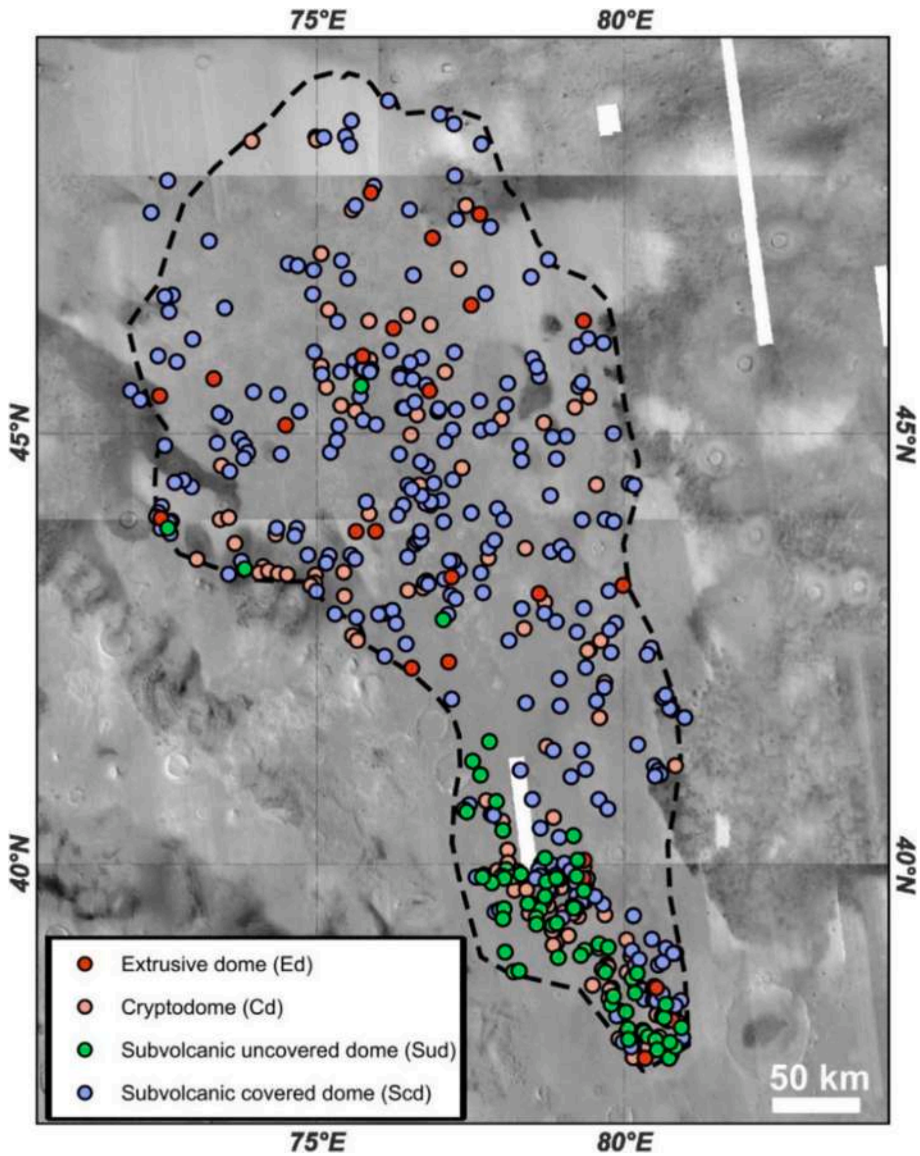

Fig. 3. Distribution of domes in the area. The four types are represented in different colors. The basemap is the global CTX mosaic.

reflectance; an atmospheric, ratio shift, and smile correction were applied to them; and they are also map-projected (Seelos et al., 2024). The cubes have an average spatial resolution of 18 m/pixel, and they cover the 436–3896 nm spectral range across 489 bands (Seelos, 2016). An additional cube was also provided within this dataset, which contained 60 spectral indexes refined for mineral recognition (Viviano et al., 2014). Finally, we retrieved spectral signatures from the NASA RELAB spectral database (Scholes et al., 2021), to compare with spectra extracted from the CRISM cubes. A comprehensive list of all the data used can be found in Annex 1.

4. Methods

4.1. Data correction and projection

Datasets from other authors, such as global mosaics, were ready for analysis, but the HiRISE and CTX images required further processing. Both products were calibrated and map-projected using the Integrated Software for Imagers and Spectrometers (ISIS) (Laura et al., 2023), and the Geospatial Data Abstraction Library (GDAL) (Rouault et al., 2023). The image processing included: radiometric correction, noise correction, image stitching, map projection, and format transformation. A detailed description of the commands used in this process can be found in Annex 2.

4.2. Mapping techniques and cluster analysis

Given the size difference between the individual domes and the study area, we decided to map at two scales with different goals. The first objective was to create a regional map to describe the floor units across the area, allowing us to understand the geological setting of the location and how the domes interacted with it. Subsequently, a detailed mapping of a single dome was done, we chose a dome that was covered by both HiRISE and CRISM datasets. Since the available spectral information was generally not conclusive, most of the units were mainly defined by their geomorphology. Nevertheless, when the spectra were clear and relevant, the units were first created as geomorphological, and later refined or modified according to the spectral information (e.g. Aileen Yingst et al., 2023; Wright et al., 2024). We defined the temporal relationships of the units by analyzing cross-cutting relationships, and when possible, we used the crater size-frequency counting technique to obtain relative ages (Neukum et al., 2001). We used the production

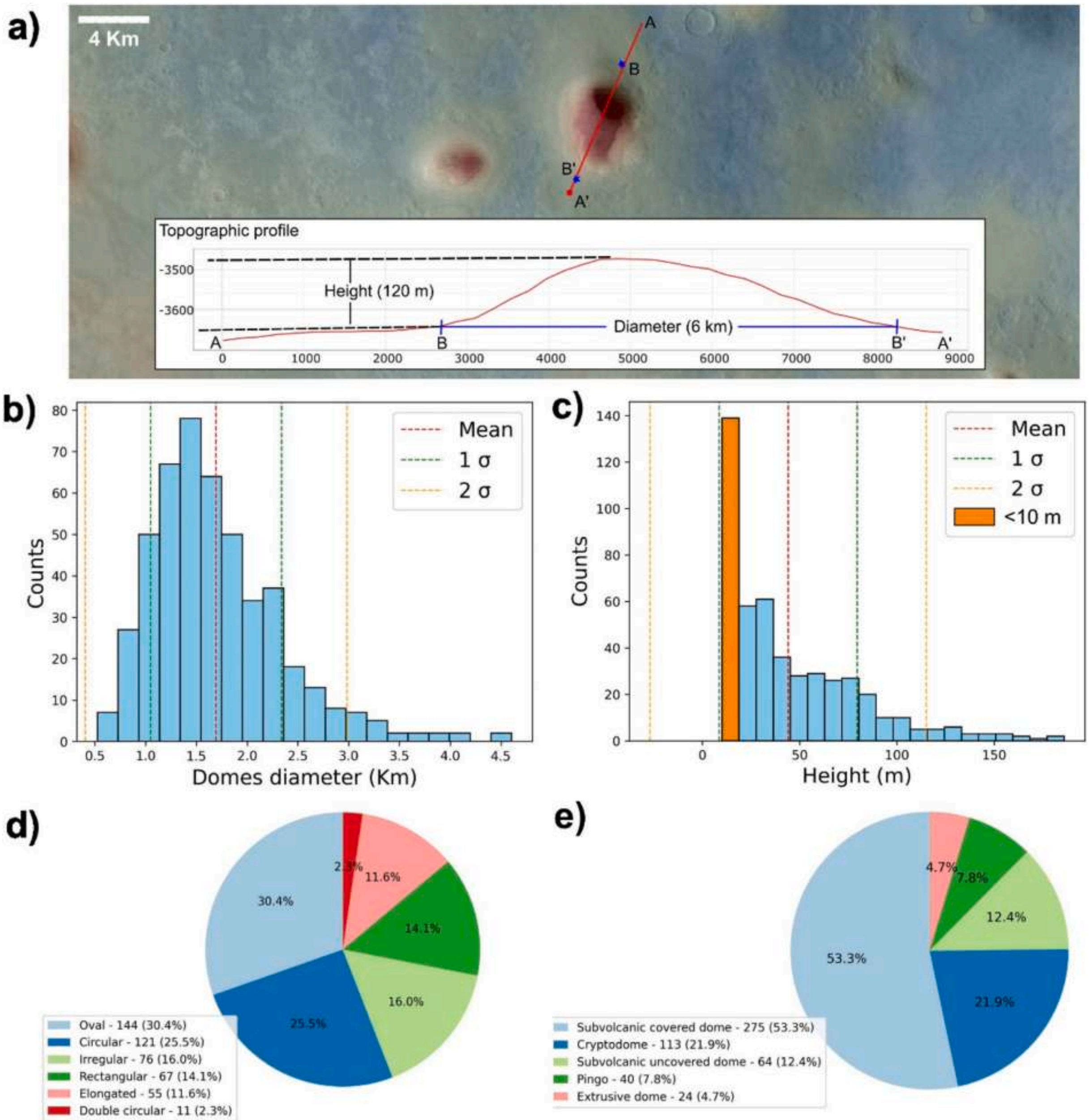

Fig. 4. General statistics of the domes. a) Methodology to measure the diameter and height of the domes. b) Histogram showing the diameters of all the domes. c) Histogram showing the height of the domes, the orange bar corresponds to the domes that were too small to be measured in the DEMS, so we assigned a value of 10 m. d) Pie chart showing the main shapes the domes can have. e) Pie chart of the percentage of domes according to their type.

function of Hartmann and Daubar (2017), and the epoch boundaries of Michael (2013). To check the distribution of the counted craters we did a Nearest Neighbor Analysis (NNI), we obtained values bigger than 1 for the Nearest Neighbor Index (*R),* meaning the data is dispersedly distributed, and thus, was suitable for the analysis (Annex 3). The analysis and mapping of the area were done in QGIS with the aid of the Mappy plug-in (Penasa and Brandt, 2021), the crater counting was performed with the CraterTools extension of ArcGIS (Kneissl et al., 2011), and the age determination was computed in the Python version of the software CraterStats (Michael, 2021).

Given the large number of individual domes, we analyzed their spatial distribution in order to identify clusters and alignments that could suggest a tectonic control on the intrusions. We followed the methodology of Hencz et al. (2023) and Le Corvec et al. (2013), which involves several steps using the programming language Python and the geoprocessing software QGIS (Annex 4). We used the global catalogue of Knapmeyer et al. (2006) to retrieve the faults in our region.

4.3. Spectral analysis

To obtain spectra from the CRISM cubes and compare them with laboratory-obtained spectra we used Python libraries that are designed for spatial analysis, specifically *xarray* (Hoyer and Joseph, 2017) and *rasterio* (Gillies et al., 2013).We also used common operational libraries like *numpy* (Harris et al., 2020), and plotting ones like *matplotlib* (Hunter, 2007). We tried to implement the signal-enhancing method suggested by Horgan et al. (2020), this process is based on the common practice of dividing the spectrum of the target area by the one of a neutral one (e.g. Pelkey et al., 2007), but in this case, the neutral area is automatically defined by setting thresholds to some of the spectral parameters defined by Viviano et al. (2014). Unfortunately, the CRISM cubes over Utopia Planitia show little spectral variation, so this method

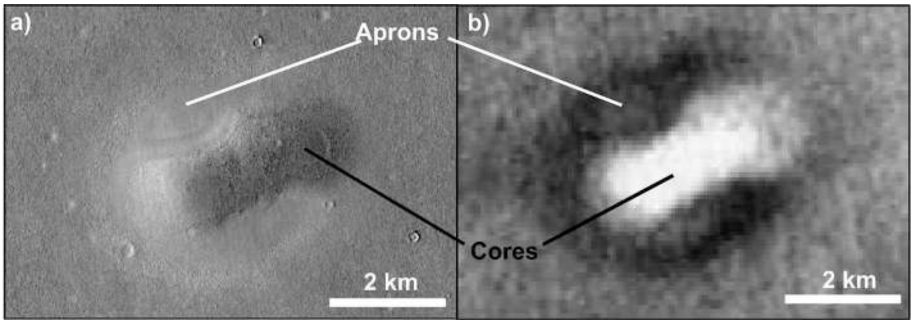

Fig. 5. Dome with a lobate structure (center coordinates: 41.83°N, 78.95°E). a) The dome as seen in the CTX mosaic, it has a central core and surrounding aprons. b) THEMIS nighttime image, the core in warmer, implying consolidated rock, while the aprons are colder, suggesting unconsolidated materials.

would diminish the spectral properties instead of enhancing them. For this reason, we decided to take the data directly from the MTRDR reflectance cubes, without spectral rationing. We also tried an unsupervised clustering analysis to obtain spectral endmembers, following the pipelines of Baschetti et al. (2024). However, the cubes were too noisy and homogeneous, so we did not obtain conclusive results. Nevertheless, we modified and used the pipelines of Baschetti et al. (2024) for plotting and analyzing the spectral signatures. Five domes were covered by the six CRISM cubes available in our area, of those, the dome showcased in the FRT00017160 had the best quality. This dome was also covered by the ESP_016944_2255 HiRISE image, so we used this data to create a detailed map of this dome. All the spectra used in this study were averaged using a 5 × 5 window.

5. Results

5.1. General details of the domes

The first step of this work was to identify all the domes within the area, describing their morphology and measuring their diameter and height. The distribution of the domes can be seen in Fig. 3, and their measurements in the supplementary materials (Suárez-Valencia et al., 2025). The morphological classification of the domes and their aprons was done using the global CTX mosaic, and the measurement of heights using the MOLA-HRSC DEM, and DEMs derived from CTX and HiRISE images when they were available.

General statistics of the domes can be seen in Fig. 4, the diameter and height were measured within QGIS. The diameter of the structures was defined as the distance between the two slope breaks between the domes and the surrounding plains (Fig. 4a). The mean diameter of the cores is 1.6 km, and they range normally between 300 m and 4.6 km (Fig. 4b). The height of the domes was defined as the difference between the

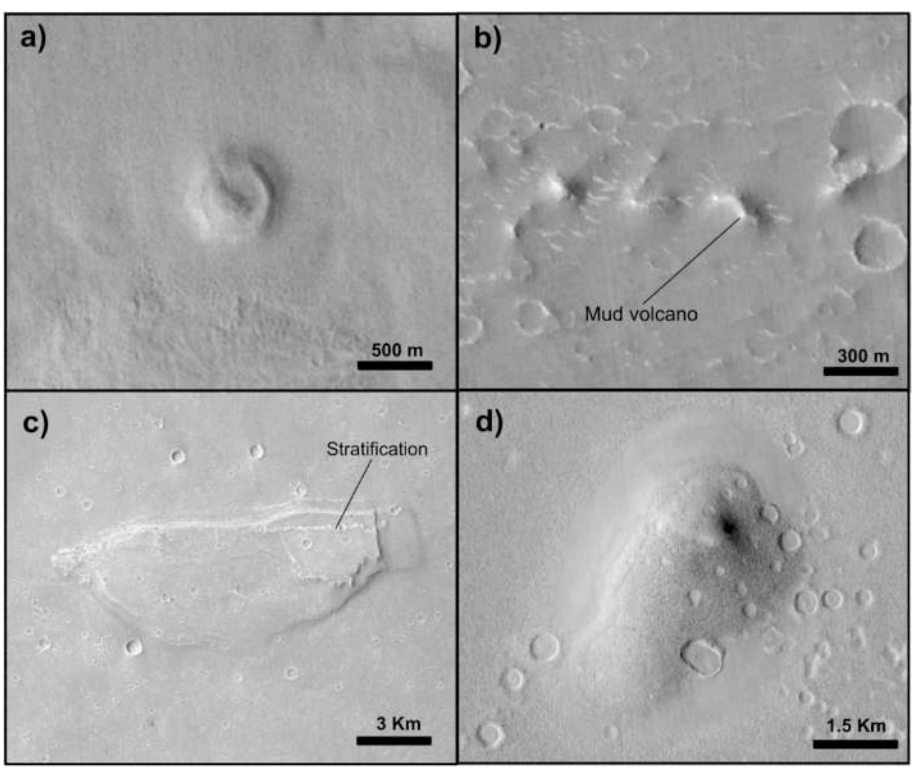

Fig. 6. Different dome-like structures found across Utopia Planitia. a) Pingos (Ivanov et al., 2014), b) A common shape of mud volcanos found in the Vastitas Borealis Formation (Ivanov et al., 2014), c) Mesas, this one showing stratification (Zhang et al., 2023), d) one candidate intrusive dome in our study area. The source image is the CTX mosaic (center coordinates: 42.59°N, 78.12°E).

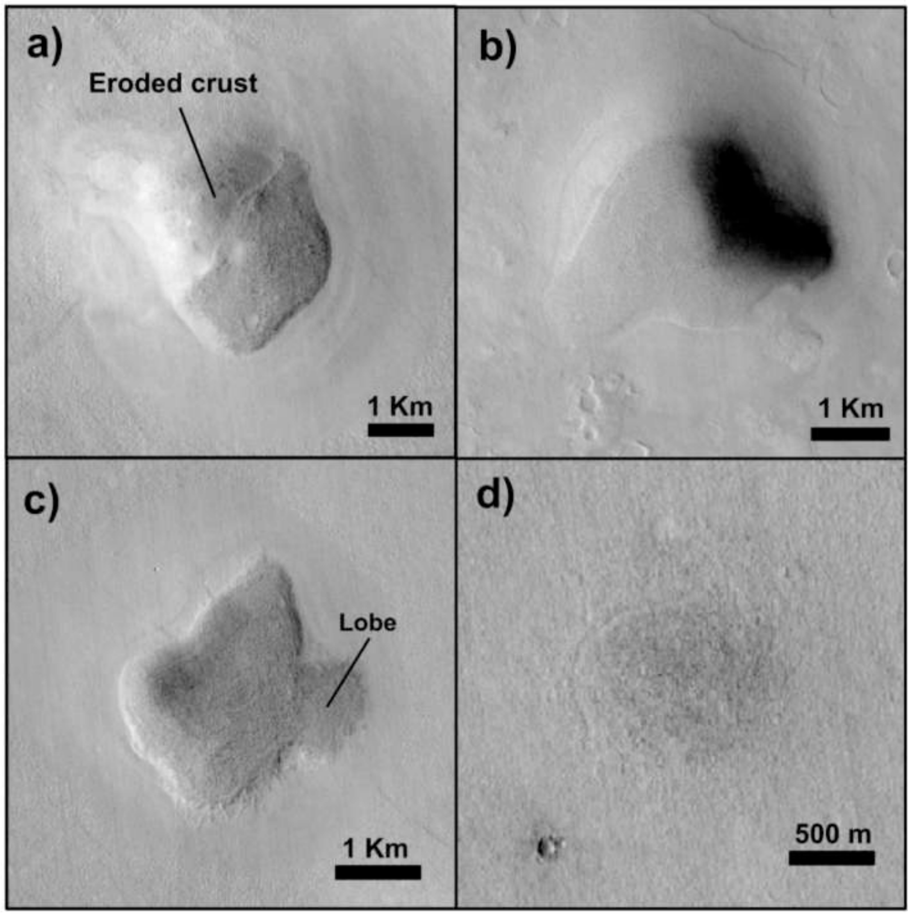

Fig. 7. Different types of domes found in the area. The source images are the CTX mosaic. a) Subvolcanic uncovered dome, with half of its crust eroded or removed (center coordinates: 42.83°N, 77.05°E). b) Subvolcanic covered dome, the covering crust is complete, also the dark coating is visible over the dome (center coordinates: 44.79°N, 75.23°E). c) Extrusive dome, with a lobe flowing over its east flank (center coordinates: 40.04°N, 79.34°E). d) Cryptodome, completely covered by the host unit (center coordinates: 39.51°N, 78.73°E).

highest point on top of the structure and the elevation of the surrounding plains, defined by the first slope break. The measurements were done using the topographic profile tool of QGIS (Fig. 4a). When possible, we retrieved the height from the DEMs derived from CTX and HiRISE images, and for the rest, we used the MOLA-HRSC DEM. Some small domes were not covered by the high-resolution DEMs, and the profiles on the MOLA-HRSC DEM were not conclusive. In those cases, we checked the MOLA individual altimetry readings (PEDR) instead of the DEM. If a point was on top of the dome, we measured its difference with the nearest point over a plain. If not, we assigned a reference value of 10 m, since the domes still cast a shadow in the CTX mosaic, indicating there is a small topographic elevation. The measured domes are on average 55 m high (Fig. 4c). Most of them are round or oval-shaped, while a minor number are irregular or rectangular-shaped, all of them have round edges (Fig. 4d). There is a significant concentration of smaller domes to the south (around 20 m high), while to the north the domes are wider and larger (between 50 and 120 m high).

An important difference with the domes on Arcadia Planitia is the lack of aureole, in this case the aprons rest next to the cores, but deposits located further away are not commonly present. The domes and their aprons are largely affected by glacial and periglacial processes, which are common in these martian latitudes (e.g. Lefort et al., 2009; Soare et al., 2013; De Pablo and Komatsu, 2009; Soare et al., 2015), the most relevant is the formation of brain terrain over the aprons of most of the domes in the region. The thermal response of the structures is like the one of the domes on Arcadia Planitia (Farrand et al., 2021), in the THEMIS nighttime image, the cores show warmer temperatures than the surrounding plains, implying solid rock or coarse materials, while the aprons have low temperatures even compared to the floor units, suggesting they are made of unconsolidated finer materials (Fig. 5). The domes are emplaced across several floor units, meaning their origin is independent of them. Most of the domes have part of their flanks covered by a black coating, this material appears to be surficial and accumulates mainly in the northeast-facing slope of the structures.

A major question regarding the nature of igneous-originated domes is how to differentiate them from other dome-forming processes. To solve this question, it was necessary to compare the domes with other similar structures. Pingos (Fig. 6a) are commonly found in these latitudes of Utopia Planitia, but they are considerably smaller than the candidate igneous domes, they are also flat-topped and have steep edges, while the domes have a convex summit and have moderate slopes (Burr et al., 2009). Another common small-sized features are mud volcanoes (Fig. 6b). Their morphology is variable, some of them have clear pits on their summit (e.g. Ivanov et al., 2014; Pondrelli et al., 2011), while other show knobs with no visible pits (Komatsu et al., 2016). However, mud volcanoes usually have diameters ranging between 50 m and 1000 m, which are consistently smaller than our candidate domes (Fig. 4a). Mud volcanoes without summit pits are not as common, they could be result of mud laccoliths (Guliyev et al., 1996), resulting in structures like igneous domes. Nevertheless, this scenario is unlikely for the domes in Utopia Planitia, given their size, shape homogeneity, large spatial span, and association to large tectonic patterns.

The distinction between igneous domes and structures formed by erosion is more challenging. Mesas, like the ones in southern Utopia

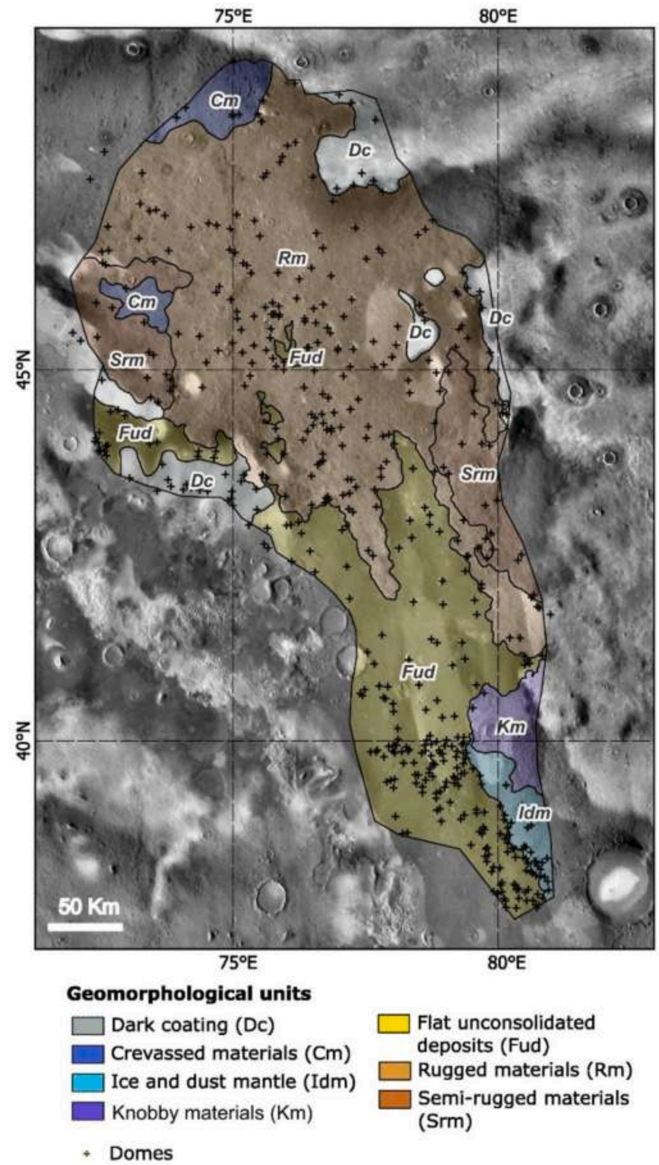

Fig. 8. Geomorphological map of the floor units in the area. The basemap is the THEMIS day infrared mosaic.

Planitia (Zhang et al., 2023), and mounds like the ones in Oxia Planum (McNeil et al., 2022), are particularly similar in size and texture to our candidate igneous domes, and they are also often accompanied by aprons. Nevertheless, these structures tend to be more angular than igneous domes, they also have rough edges, flat summits and are usually made of multiple layers of rocks. Subtle stratification can also be identified on their walls and summits (Fig. 6c). In contrast, the domes in Utopia Planitia have soft edges, most of them are round-shaped, and they all have convex summits without any kind of stratification. Having discarded the previous options, we classified our domes as igneous in origin (Fig. 6d).

Although all the domes share the previous characteristics, they were classified in subclasses according to their morphological properties (Fig. 3, Fig. 4e). The most common type is the "subvolcanic covered domes" (***Scd***), these structures are like the ones studied in Arcadia Planitia by Farrand et al. (2021) (Fig. 7a). They are the largest type of domes (larger than 1 km), their cores are clearly distinguishable from the host units, and they are made of closely packed blocks with diameters ranging from 3 to 6 m (Fig. 2c). The cores can have several shapes, from circular to irregular (Fig. 7). The aprons are generally well-developed, extending hundreds of meters away from the cores. These domes do not have lobes or vents associated with them, and their texture is homogeneous. The domes in the "subvolcanic uncovered domes" (***Sud***) type are generally smaller (sizes less than 1 km), the shallowest layers of their cores are partially removed, potentially uncovering the rocks below (Fig. 7b). They are mainly circular-shaped, and sometimes oval-shaped. Some of them have large aprons like the previous type, others have ejecta-like deposits around them, and others do not show aprons at all. "Extrusive domes" (***Ed***) are similar in size and texture to the subvolcanic covered ones, but they have well developed lobes next to the core, and/or summit pits. The lobes appear to be formed by viscous materials, since they do not spread far away from the domes or are clearly detached from them (Fig. 7c). Finally, the "cryptodomes" (***Cd***) type are equivalent to the features of the same name described by Rampey et al. (2007) in Arcadia Planitia, these structures do not have cores or aprons, they are small and usually circular (Fig. 7d). Cryptodomes have no effect on the continuity of the host unit, meaning the intrusive body is buried near the surface, like a laccolith (Schofield et al., 2021).

5.2. Floor units

The floor units in the study area have diverse origins due to their position near the northern martian dichotomy (Ballantyne et al., 2023). A map with the geomorphological units on the area is shown in Fig. 8. The largest unit is "Rugged materials" (***Rm***), it is characterized by a rugged texture, high albedo, and low thermal inertia. Periglacial landforms are common, including scallops, crevasses, polygons, large-scale pits, and occasionally brain terrain, the last mainly associated with the aprons of the domes. These structures have been described extensively by previous authors in studies of nearby locations, they are thought to be formed by seasonal thermal contractions of ice-rich soils and the interaction of these layers with sunlight, atmospheric, and gravitational processes (e.g. Soare et al., 2015; Lefort et al., 2009; Haltigin et al., 2014).The aprons developed in this unit are usually incomplete due to the development of scallops or polygons over them. This unit correlates spatially to the Astapus Colles unit defined by Tanaka et al. (2005).

The second largest unit is the "Flat unconsolidated deposits" (***Fud***), it is located south of the ***Rm*** unit and extends to the outskirts of the Nilosyrtis Mensae. This unit is almost flat, although at a regional scale it is gently dipping towards the center of the basin. It has high albedo and the highest thermal inertia in the region. It is the lowest unit in the area, having discordant contacts with the surroundings ones, which suggests it is filling a local low. Internally, the unit is made of blocks ranging from 1.5 to 5 m in diameter, spread across a matrix of finer-grained material. Periglacial landforms are less common in this unit, which in turn allows the aprons of the domes to be well developed and continuous. Some sinuous rilles cross the area, they are filled by materials that are massive, or that have a grain size smaller than the image resolution (here denominated fine-grained materials). Some domes are superimposed to the rilles, locally interrupting their continuity (Fig. 9a). We also identified the silhouettes of buried craters, meaning the unit may be covering a basement below. This unit correlates spatially with the Utopia Planitia 2 unit of Tanaka et al. (2005).

To the southeast lies the "Ice and dust mantle" unit (***Idm***), it has the smoothest texture of the units in the area, high albedo, and high thermal inertia. Periglacial and sublimation landforms are common. Its surface is heavily pitted, and brain terrain develops frequently. It is composed of fine-grained or massive materials. It appears to be superimposed to the ***Fud*** unit, having lobate flow-like contacts with it. Crevasses are common, as well as large sublimation pits and polygons. The domes emplaced in this unit lack aprons, and some have flow structures surrounding them (Fig. 9c). This unit matches the description of the Amazonian dust-ice mantle described by Soare et al. (2012), as well as the Vastitas Borealis marginal unit of Tanaka et al. (2005).

Another set of units seems to be modified portions of the ***Rm*** unit,

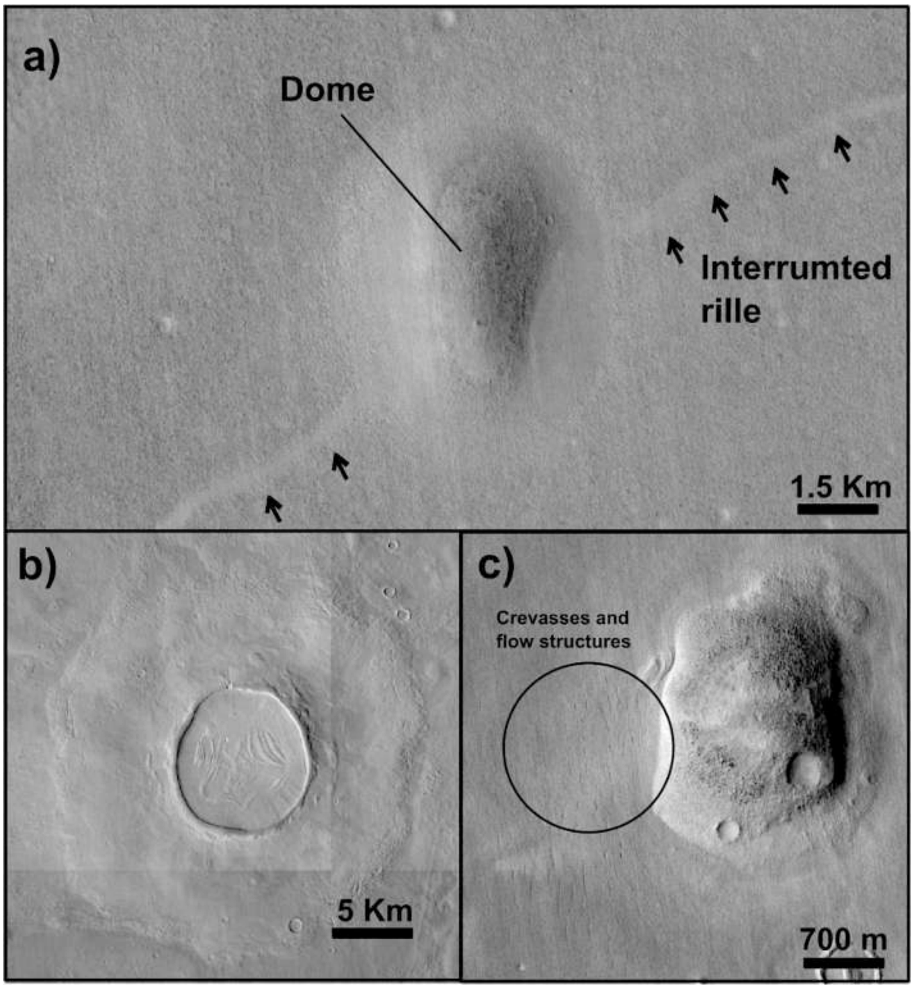

Fig. 9. Notable landforms on the floor units. The source images are the CTX mosaic. a) Dome superimposed to a rille in the ***Fud*** unit, suggesting they dome is younger (center coordinates: 41.09°N, 79.37°E). b) Pancake-type crater in the ***Idm*** unit (center coordinates: 40.10°N, 79.86°E). c) Flow structures surrounding a dome in the ***Idm*** unit (center coordinates: 39.12°N, 80.45°E).

probably by glacial and periglacial activity. The "Knobby materials" unit (***Km***) is just north of the ***Idm*** unit, it has a rough texture and high albedo. It contains large knobs that appear to be covered by a mantle of ice and dust. Craters in this unit are usually pancake-type (Fig. 9b). The unit "Semi-rugged materials" (***Srm***) appears at the west and east borders of the area. It has a rugged texture in some locations, and smooth texture in others. This unit could also be related with the suit of periglacial landforms described by Soare et al. (2015). The unit "Crevassed materials" (***Cm***) is in the northernmost part of the area. It is characterized by the presence of large arc-shaped crevasses. The prior units are also spatially concordant with the Astapus Colles unit of Tanaka et al. (2005).

Finally, there are large areas covered by a "Dark coating" (***Dm***); these layers appear thicker than the ones over the flank of the domes (Fig. 2b, Fig. 7b). Apart from the lower albedo, its other morphological characteristics are like the ones of the ***Fud*** unit. In specific locations, "spiders" are formed within the dark coating materials (Reiss et al., 2016).

5.3. Crater counting

We performed a crater-counting analysis over the three larger floor units in the area: ***Fud***, ***Rm***, and ***Idm***. The analysis retrieved an age of 2.36 ± 0.15 Ga for the ***Fud*** unit, 2.77 ± 0.32 Ga for the ***Rm*** unit, and 1.21 ± 0.17 Ga for the ***Idm*** unit (Fig. 10).

The age obtained for the ***Fud*** unit probably represents its formation age, since this unit does not appear to have been highly reworked by posterior process. That is not the case for the ***Rm*** and ***Idm*** units. Both units are characterized by the presence of glacial and periglacial features which appear to have modified the surface to a large degree, erasing a large number of craters from it. Hence, we consider these two estimations as resurfacing ages related to the beginning of large periglacial activity, and not the deposition ages of the materials that compose the bulk of these units. Given these constrains, we defined the temporality of events mainly from the stratigraphic relationships between units, and used the ages derived from this analysis as constraining times for the igneous activity.

5.4. Detailed map of a dome

We conducted a detailed mapping of an irregular dome and its surroundings in the ***Rm*** unit (Fig. 11). It was selected because it is covered by both the ESP_016944_2255 HiRISE image and the FRT00017160 CRISM cube. The core of the dome is 5.44 km in diameter in its largest direction, 2.54 km in the shorter one, and it is 156 m high.

The Dome core (***Dc***) is an oval-shaped hill that stands out from the plain. Its texture is homogeneous. Its surface is dominated by blocks ranging from 3 to 6 m in diameter, closely packaged in a matrix of fine-grained materials (Fig. 12a). The spectral signatures of the dome core show the three absorptions bands of olivine at 1 μm (Burns, 1993; Viviano-Beck et al., 2014), although the bands are shifted to shorter wavelengths, probably due to the presence of pyroxene (Fig. 13a). This

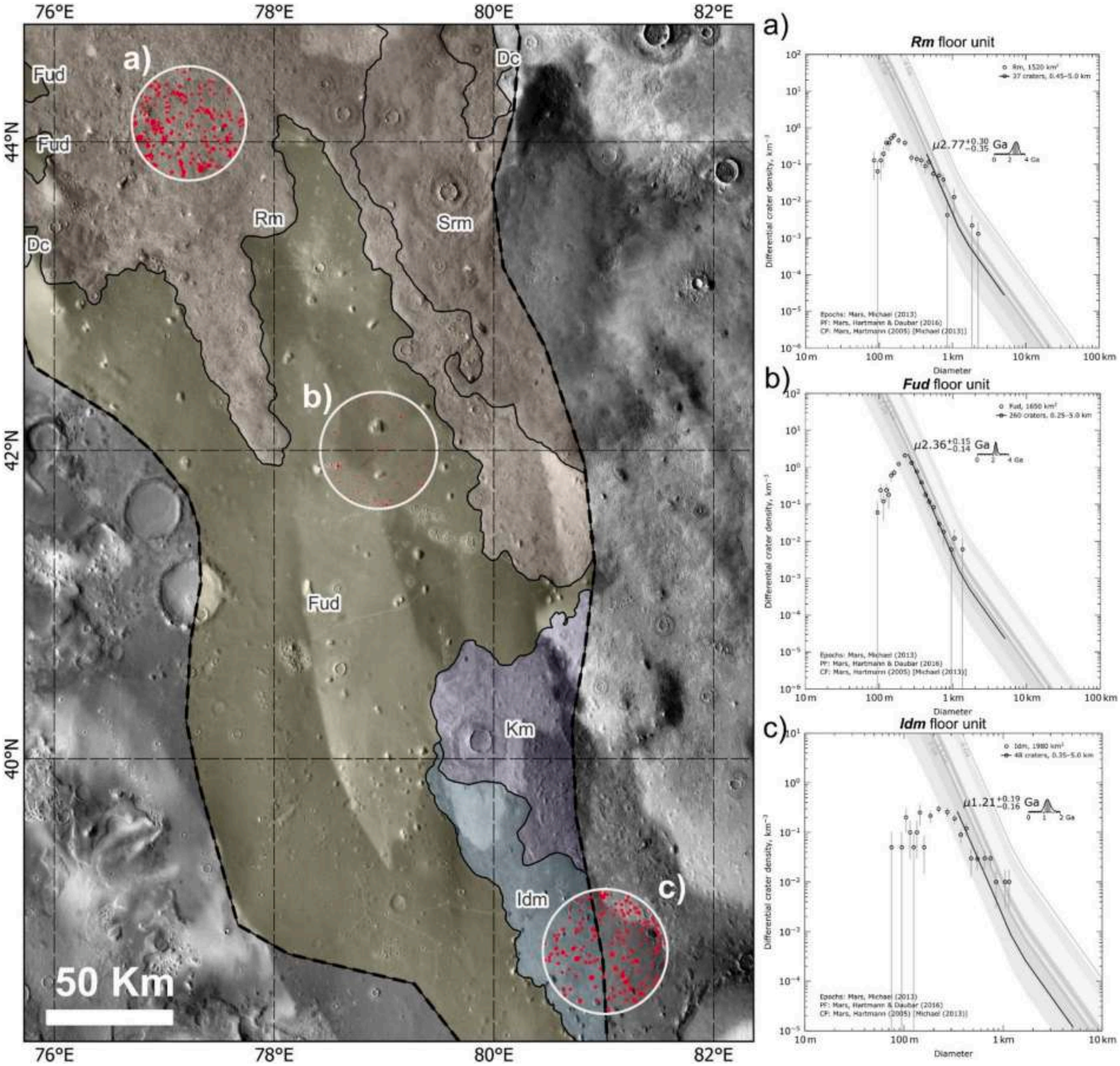

Fig. 10. Crater counting analysis. a) The results for the ***Rm*** unit, retrieving an age of 2.77 ± 0.32 Ga. b) The results for the ***Fud*** unit, retrieving an age of 2.36 ± 0.15 Ga. c) the results for the ***Imd*** unit, retrieving an age of 1.21 ± 0.17 Ga. The basemap is the global CTX mosaic.

composition could correspond to basaltic rocks, but the signature on the surrounding units gave a similar result, this homogeneity could indicate that the measured spectra belong to a surficial material covering the whole area, and not to the units themselves. Considering the presence of dunes and other aeolian features, these signatures might be related to a layer of basaltic sands. A small portion of the dome is covered by a fine-grained or massive material (***Cd***), probably a shallow layer of dust and ice. To the south, brain terrain is developing over this unit. A small tongue-shaped lobe is visible in the left flank of the dome (***Dl***), the materials flowed downslope a couple of meters. This is probably related to a gravitational process.

The aprons of the dome are divided into two regions. First, next to the core lies the Covered Aprons (***Ca***), this unit fully encircles the dome and it is located close to the slope break with the floor unit. The materials of the dome are not visible, instead a fine-grained material covers a slightly bulged terrain. Traces of sediments moving down the slope of the dome and incipient brain terrain are common in this unit. Further away is located the hardly distinguishable Distal Aprons unit (***Da***), it is a semi-circular region outside of the ***Ca*** unit made of fragments that are 3 to 4 m wide, which are scattered over the floor unit. This region may be the equivalent to the aureole described by Farrand et al. (2021). Brain terrain can also be found over some aprons and parts of the floor unit (***Bt***) (Fig. 12b). The polygons conforming the brain terrain are smaller near the boundary with the ***Ca*** unit, which appear to be gradually transforming into ***Bt***.

The floor unit in this location is Rugged materials (***Rm***), its surface is characterized by polygonal structures and incipient brain terrain. There are no large sediments over it, the covering material is either fine-grained or massive. Its spectral signature is homogenous, it has a broad absorption at 1 um and no more clear absorptions, similar to the spectrum of the dome core (Fig. 13a). Over this unit several scallops develop (***Sp***), these landforms are made of a scarp on one side, and a gentle slope on the opposite one (Fig. 12c) (Lefort et al., 2009). Brain terrain is commonly found in the inner part of the scallops. A couple of pingos were also identified in the location, one is a small tongue-shaped structure with steep edges (***Pg***), while the other is a flat-topped pingo (***Ftp***), more oval-shaped and with a smoother surface (Dundas and McEwen, 2010).

The most contrasting feature of the location is a dark coating that covers the northern part of the dome and some portions of the floor unit

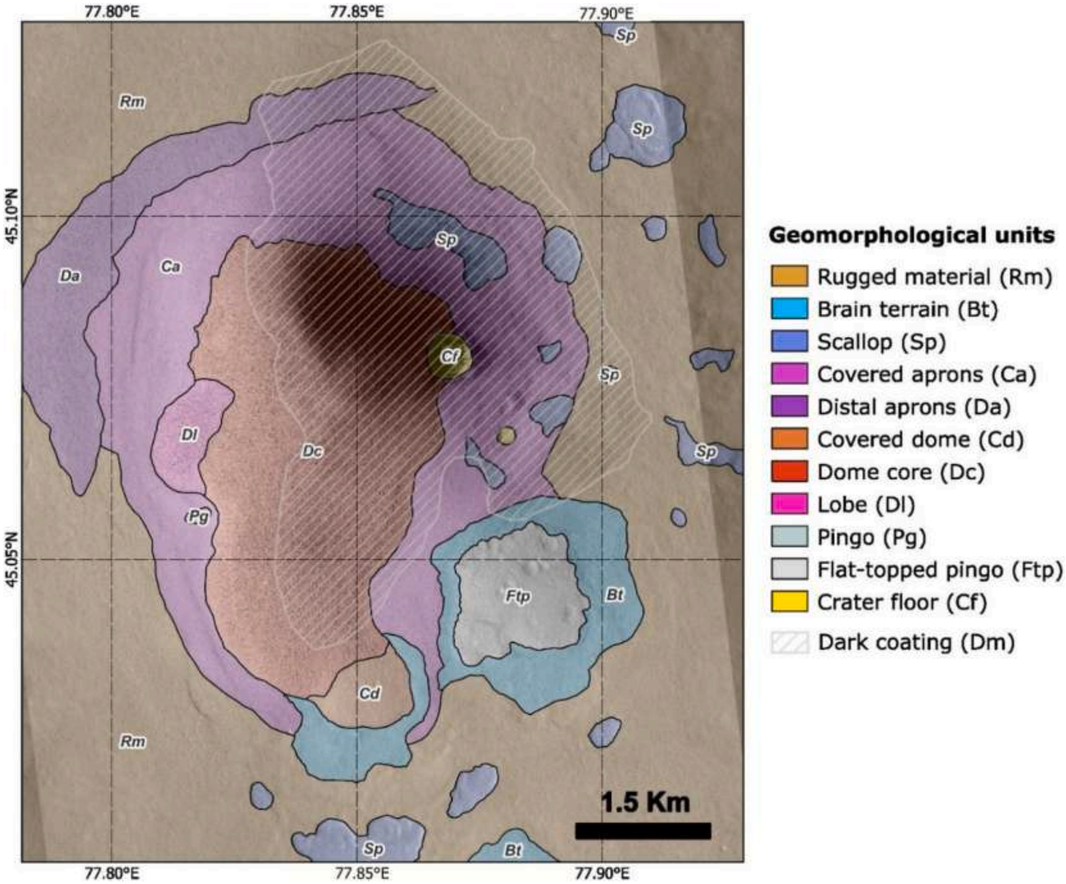

Fig. 11. Geomorphological map of a subvolcanic covered dome in the ***Rm*** floor unit. The basemap is the ESP_016944_2255 HiRISE image (center coordinates: 45.07°N, 77.84°E).

(***Dm***). The material is superficial, since scallops, rock fragments, and other underlying structures are visible through it (Fig. 12d). This unit appears green in the FM2 RGB composite of Viviano-Beck et al. (2014) (Band depth at 530 nm, Band depth at 920 nm, and the Integrated band depth a 1 μm), which suggests it contains coarse-grained Fe minerals (Fig. 12b). Its spectral signature also has a negative slope after 1 um (Fig. 13a), which has been related to ferric coatings and nanoparticle iron (Viviano et al., 2014). Other domes in the region have similar accumulations of dark material, usually in the same northeast-facing flank. This implies that this material is being deposited by a regional process.

5.5. Distribution analysis of the domes

Volcanic fields are usually related to the tectonic configuration of the location they are intruding, since the upwelling magma would take advantage of faults and fractures to reach the surface. To evaluate if that was the case in Utopia Planitia, we made a distribution analysis of the domes and compared it with the local faults. Before the analysis, one should determine if the domes are randomly scattered or clustered. This was done applying a Nearest Neighbor Analysis (NNA) to the domes (Le Corvec et al., 2013), which measures the distance between each dome and their closest neighbor, and then compares that distance with the expected one for a random distribution. The result of the NNA is interpreted with the Nearest Neighbor Index (*R)*, which will be greater than 1 if the distribution is random, and smaller if they are clustered. The value of *R* for the domes in Utopia Planitia is 0.83, indicating that the domes are clustered. The code used for this process can be found in the supplementary materials (Suarez-Valencia et al., 2024).

After confirming the clustered nature of the domes, the next step was the generation of a heatmap. This technique has been used before in volcanic settings to check for spatial concentrations of volcanic features (Trippanera et al., 2018). The heatmap in Fig. 14 was produced with the homonymous tool in QGIS, using a 50 km search radius. Two major dome clusters were found in the southern part of the region. Both clusters are dominated by the ***Sud*** type of domes, which are also almost restricted to this location. The clusters are located over the ***Fud*** unit. Smaller concentrations can be found in the northern part of the region, especially over the central ***Rm*** unit, in this case the dominant type of dome is ***Scd***.

To identify if the domes are related to any tectonic pattern, it was necessary to check if they are aligned along preferential directions (e.g. Cañón-Tapia and Jacobo-Bojorquez, 2022). We followed the methodology of Hencz et al. (2023), which consists of creating lines that connects each dome with the others, to later analyze the lines that connect more than two domes. The elongated shape of the dome field could affect this analysis, since the lines along the longer axis have a bigger chance of crossing more than two domes. To avoid this effect, we created three 100 km circles in the north, center and south parts of the area (Fig. 15). Only the domes inside each circle were computed in the analysis, restraining the effect of long lines between far away domes. This process was done in Python and QGIS. Although not every three-dome alignment has to be necessarily related to a tectonic feature, multiple alignments on a large dataset may represent regional trends.

The obtained lines and rose diagrams for each sub-area are shown in Fig. 15. Across the three groups, most of the lines follow a NW-SE trend. Since the direction is consistent across the spatially separated groups, it is possible to assume that this alignment is related to a geological feature. We have further evidence of this by considering the trend of the regional faults system derived from Knapmeyer et al. (2006), which also follows an NW-SE trend (Fig. 15d).

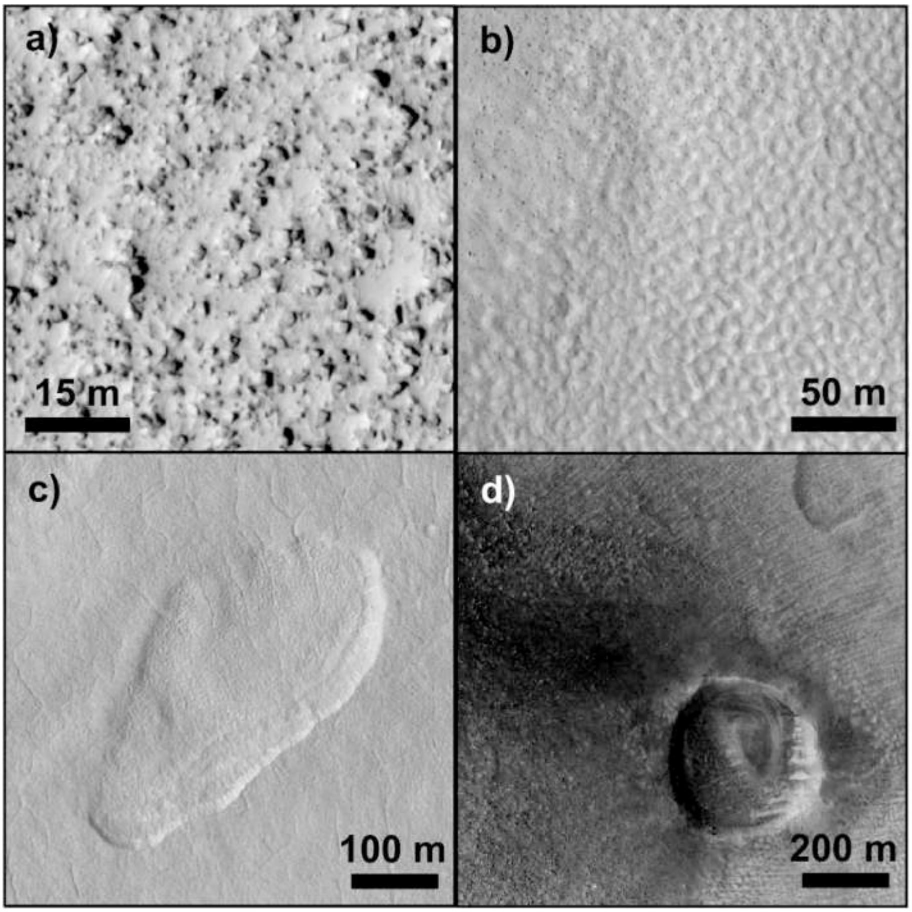

Fig. 12. Outstanding landforms near the dome mapped in detail, from the ESP_016944_2255 HiRISE image. a) Texture of the dome core (***Dc***), made of closely packaged blocks, b) brain terrain advancing over the aprons (***Bt***), c) typical scallop (***Sp***), d) a crater visible through the dark coating (***Dm***).

6. Discussion

6.1. Stratigraphic position of the domes

Since the domes are present all over the area, establishing their stratigraphic relationship with the floor units was challenging. However, we found that their relationships with minor structures and the status of the aprons were helpful clues. In the case of the domes located in the ***Idm*** unit, we found that the aprons are absent, they are more likely buried beneath deposits of ice and dust (Fig. 16a). Flow patterns are seen around some domes, as well as crevasses and pits, this suggests that these flows are glacial masses that are pushing and embedding pre-existing domes (Fig. 9c). The previous patterns would only be possible if the domes were older than the ***Idm*** unit.

The situation is more complex in the ***Fud*** unit. The ***Sud*** type of domes likely postdates its emplacement. The fact that the inner materials of these domes are uncovered implies that the topping unit was eroded or removed after their intrusion, regardless of if it was made of a hyaloclastite carapace, the Fud unit itself, or a combination of both (Fig. 16b). Additionally, some Sud domes show ejecta-like deposits around them, possibly pyroclastic products (Fig. 16b), while others are superimposed over the rilles that cross the unit (Fig. 9a), further suggesting that these domes are younger than the ***Fud*** unit. Some domes of the ***Scd*** type also appear to postdate the ***Fud*** unit, since there are no flow structures around their cores and their aprons are fully developed and uninterrupted (Fig. 16c). However, other domes of the same type have hardly visible aprons, instead, the materials of the ***Fud*** unit surround their cores, generating sharp contacts (Fig. 16d). We propose that these domes were there before the ***Fud*** unit, which later embedded them. Cryptodomes are also common in this unit, they could be either pre-existing domes covered during the emplacement of the ***Fud*** unit, or posterior intrusions that stalled near the surface. We opt for the second option, since the cryptodomes are similar in size and are located in the same cluster as the ***Sud*** type, which postdates the ***Fud*** unit.

Finally, all the domes in the ***Rm*** unit appear to be younger than its formation. In most cases aprons are present, like in the dome mapped in detail (Fig. 11), and when they are not, it is usually because they were modified by more recent periglacial activity or covered by ice and dust. Furthermore, there are no signs of domes embedded by the materials of this unit.

6.2. Magmatic regime

The domes in Utopia Planitia are varied, they range from cryptodomes to extrusive domes, showing an intrusive-to-extrusive type of magmatism. Given these characteristics, the genetic model proposed by Farrand et al. (2011) for the domes in Arcadia Planitia could also be applied here. In that scenario, pockets of magma either reached the surface to create extrusive domes (***Ed***) or stalled near it to form intrusive structures. Some among the latter were uncovered by erosion or by other uplifting processes, giving place to subvolcanic domes (***Sud*** or ***Scd*** types), while the ones that remained trapped below the surface became cryptodomes (***Cd*** type).

Regardless of the type, the domes are individual edifices with homogeneous shapes, even the extrusive ones show at most one lobate feature next to them. Therefore, we believe the magmatic activity on the area had a monogenetic behavior, meaning that every dome is a single eruption or intrusion, with no further events in the same spot (Smith and

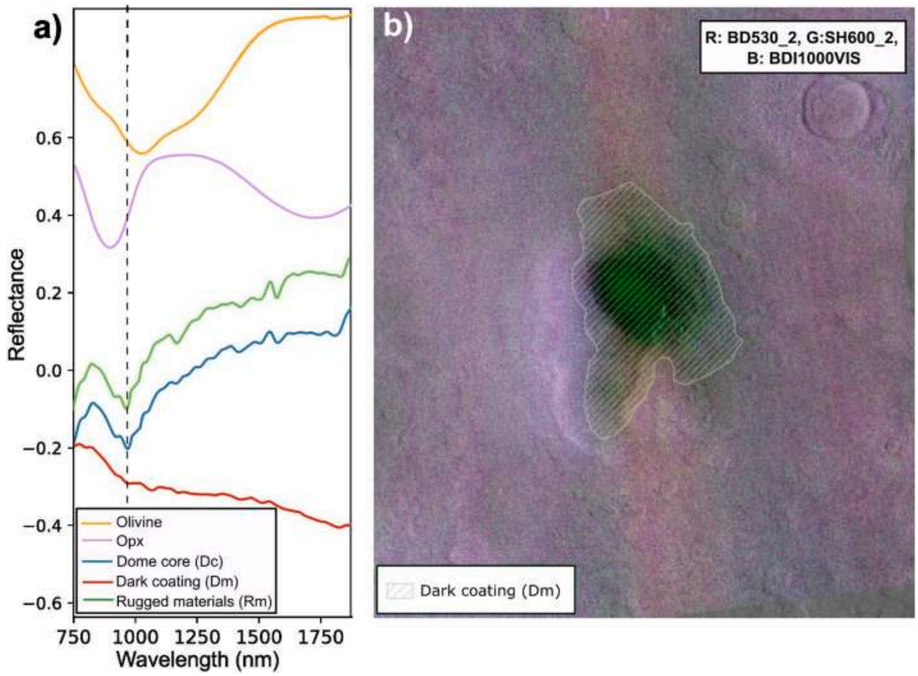

Fig. 13. Spectral signatures of the main units from the FRT00017160 CRISM cube. a) Comparison of the spectra of the units with the ones of olivine and orthopyroxene. The absorption at 1 μm of the units ***Rm*** and ***Dc*** show the three absorptions of olivine, but shifted to shorter wavelengths, probably due to the presence of orthopyroxene. The dark coating has a strong negative slope from 1 μm to the end of the spectrum around 2.6 μm. b) FM2 RGB composite, the dark coating appears green, which is consistent with Fe minerals. (For interpretation of the references to colour in this figure legend, the reader is referred to the web version of this article.)

Németh, 2017). Monogenetic magmatism is usually related to depth and small-scale sources, these systems do not widely interact with the intruded crust, avoiding the formation of magma chambers or evolved magmas. In this case, we would expect the domes to be mafic in composition, which aligns with the mineralogy observed in the CRISM cubes. It is worth mentioning that the cubes over the zone were noisy and probably heavily influenced by dust, so we cannot rule out the presence of other species being masked by it. It is also possible that the spectra measured over the domes correspond solely to the composition of the overlying dust, which could consist of olivine-rich sands transported from other locations. In this scenario, the composition of the domes themselves would not necessarily be basaltic and could instead align with the findings of Farrand et al. (2021) for the domes in Arcadia Planitia, which were classified as felsic to intermediate due to the detection of alkali feldspar.

From the heatmap, it was determined that a large cluster of domes is located south of the area (purple circle in Fig. 14), this cluster is also dominated by the ***Sud*** and ***Cd*** dome types, opposite to the dominance of the ***Scd*** type in the rest of the area. This cluster is also located exclusively over the ***Fud*** unit. Since this group of domes is spatially constrained and morphologically homogeneous, it likely represents a different magmatic event compared to the one that affected the whole region. This event would have been weaker, since the resulting domes are smaller and concentrated in a reduced area. According to (Le Corvec et al., 2013), monogenetic fields are generally clustered, and their spatial extent corresponds to a combination of the tectonic regime and the dynamic of the mantle source.

The preferential trends of the alignments of the domes imply that the parental magmas took advantage of the regional faults and structures, with a NW-SE trend (Fig. 14). Igneous systems commonly follow tectonic patterns when available, since they work as weak zones for the magma to rise (Mazzarini and Isola, 2024). Thus, we can assume that the domes in Utopia Planitia used pre-existing tectonic patterns as conduits to intrude. A diagram of how the intrusive system could work can be seen in Fig. 17. Our study area is close to the northern martian dichotomy, which could have an incidence in the emplacement of the two magmatic events. According to the models of Wieczorek et al. (2022), the crust in this location is ~40 km thick, ~20 km less than south of the dichotomy. Since the magma sources for monogenetic fields are deep, a thinner crust could facilitate the formation of such magmatic events. Although the origin of the dichotomy is still under debate, some authors suggest it could be the result of a giant impact on the northern hemisphere (Marinova et al., 2008), which would have generated an extensive system of faults that intrusions could have used to reach the surface. Regardless of the scenario, many magmatic systems were active near our area, like Syrtis Major and Nili Fossae (Mandon et al., 2020; Werner, 2009).

6.3. Geological history of the area

Since the number of magmatic events and their temporality were already established, we defined the sequence of events that configured the area (Fig. 18). The first event was the emplacement of the ***Rm*** unit, which is genetically related to the Vastitas Borealis unit described in other works (Tanaka et al., 2014; Liu et al., 2022). This unit is thought to be made of large-scale sedimentary deposits produced by an ancient ocean covering the lowlands, or by outburst flows originating in the lowlands. Given the regional nature of these deposits, it is possible that this unit also forms the basement of the whole region. According to Tanaka et al. (2014), these sequences were deposited in the Late Hesperian (~3.0 Ga). After the emplacement of the ***Rm*** unit, a magmatic event produced the first set of domes, most of them reached the surface through time, making the bulk of the ***Scd*** type. The timing of their intrusion is uncertain. The aprons of the domes developed soon after their emplacement, driven by gravitational processes, atmospheric erosion, and glacial erosion. We found small distal aprons during our detailed analysis of the dome in the ***Rm*** unit. These deposits might correspond to the aureole described by Rampey et al. (2007), but it is unclear why they are underdeveloped in the Utopia Planitia region.

Next, the materials of the ***Fud*** unit were deposited around 2.36 ±

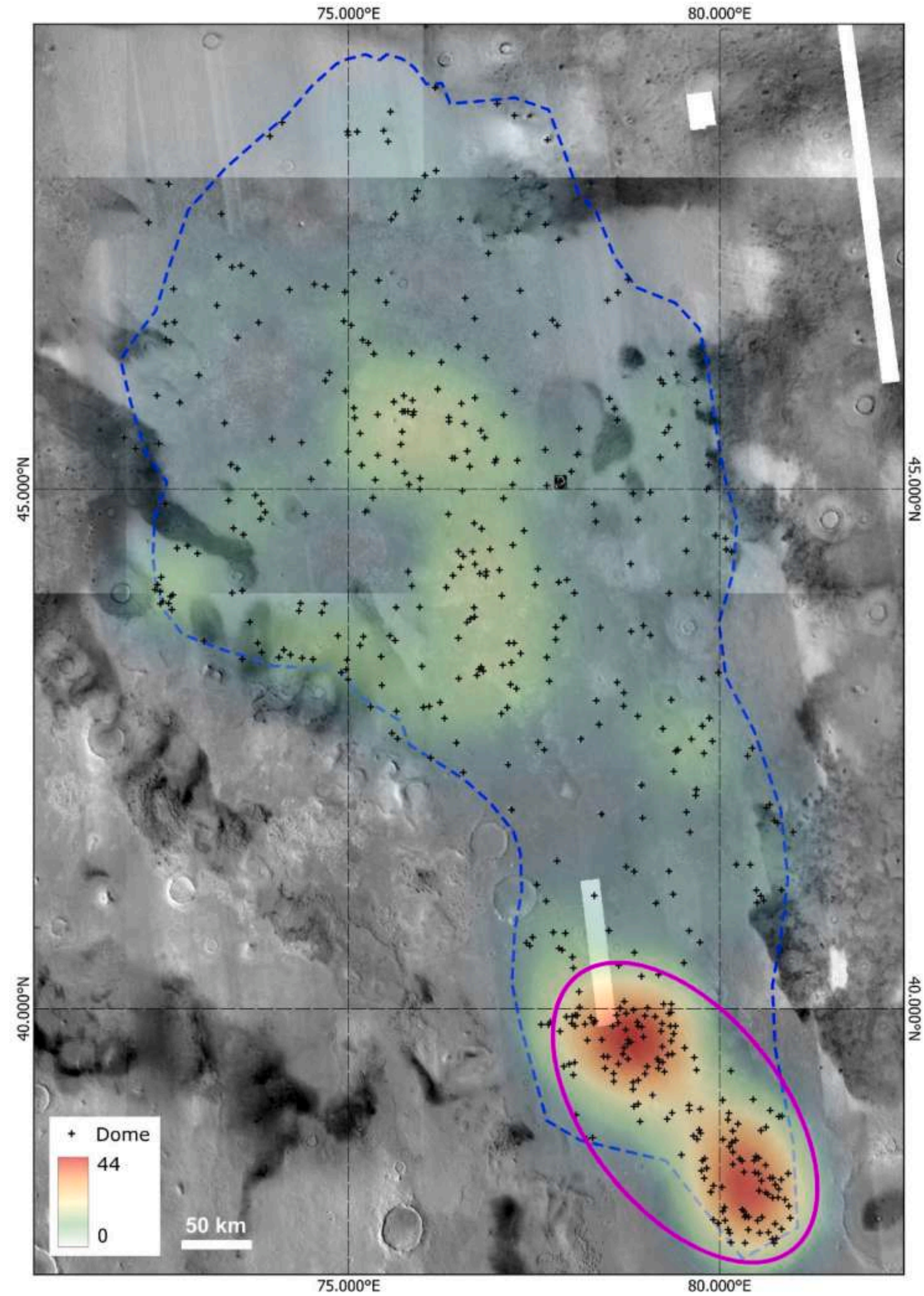

Fig. 14. Heatmap showing the concentration of domes. There is a large cluster of domes to the south of the region (purple region), which likely indicates a different magmatic pulse. The basemap is the global CTX mosaic. (For interpretation of the references to colour in this figure legend, the reader is referred to the web version of this article.)

0.15 Ga. We believe this unit is made of sedimentary deposits linked to outburst flows from the southern highlands, probably from Nilosyrtis Mensae (Bandfield and Amador, 2016). Nevertheless, those chaotic terrains could be also associated with older events, like the formation of the ***Rm*** unit. This unit mainly fills a large basin south of the ***Rm*** unit. From the analysis of the aprons we know that some domes existed before the emplacement of the ***Fud*** unit, since they were covered or surrounded by the filling material. A second magmatic event took place after, forming smaller domes that intruded through the already existing ***Fud*** unit. The sinuous rilles found in the area are probably formed by lava flows of this magmatic event. According to our calculations, the two magmatic pulses discussed here happened after the events in Syrtis Major (~3.5–3.8 Ga) (Bramble et al., 2017), and Nili Fossae (~3.82 Ga) (Mandon et al., 2020), meaning they are the youngest large-scale magmatic events in the surroundings. It is unclear why there is a temporal gap between the two magmatic events. Although single terrestrial monogenetic pulses can span timespans of ~500 ka – 1 Ma (Jaimes-Viera et al., 2018), the gap between both events in Utopia Planitia is much larger (~700 Ma), we believe that both pulses are unrelated, and that the emplacement of a second monogenetic pulse in this location respond to variations in the mantle below Utopia Planitia.

Around the same time that the second magmatic pulse was occurring, and continuing thereafter, periglacial activity significantly reworked the **Rm** unit, covering the aprons of some domes and generating subunits characterized by periglacial landforms (***Km***, ***Srm***, ***Cm***). Later, around 1.21 ± 0.17 Ga, the ***Idm*** unit was formed, likely due to large depositions

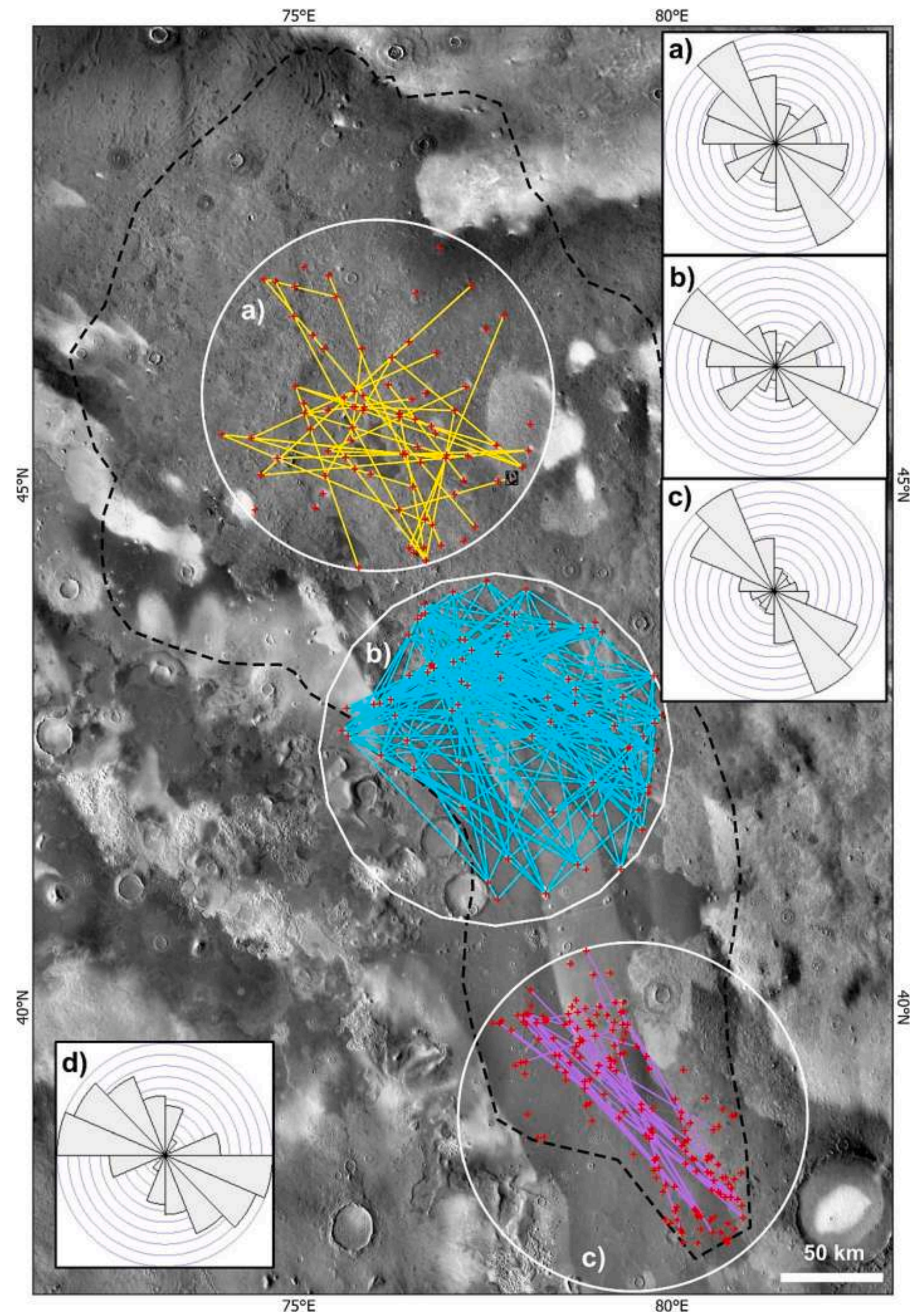

Fig. 15. Alignment analysis for three zones to the north, center, and south of the area. The lines represent alignments of more than two domes. Only some of the lines are represented for clarity. All the regions have a preferential NW-SE trend. a) Northern area and its rose diagram, b) central area and its rose diagram, c) southern area and its rose diagram. d) Rose diagram of the regional faults of Knapmeyer et al. (2006), which also follows a NW-SE trend. The basemap is the THEMIS day infrared mosaic. (For interpretation of the references to colour in this figure legend, the reader is referred to the web version of this article.)

of ice and dust (Soare et al., 2012), covering the prior units as well as the aprons of the domes in this location. Finally, the dark coatings (***Dm***), and other aeolian landforms are probably recent, since they are shallow and unconsolidated. The dark coatings usually appear in the NE-facing scarps of the domes, suggesting that they follow a regional wind trend.

7. Conclusions

The dome field in Utopia Planitia is likely igneous in origin, their morphological properties are different from other dome-like structures like pingos or mesas, and they share the general structure of the dome field in Arcadia Planitia. The edifices vary greatly in size and shape, some of them show the typical features of extrusive domes, such as lobes and summit pits, while others are buried and barely visible. This configuration indicates an intrusive-to-extrusive regime, one in which most of the domes were emplaced near the surface like laccoliths, while a smaller number of them reached the surface as extrusive domes. The magmatic regime is likely monogenetic, since the structures are homogeneous and do not show signals of recurrent eruptions or emplacements.

Two different intrusive stages were identified, which produced a set of domes with different characteristics. However, regardless of the type or timing of domes, the intruding magmas that formed them seem to have taken advantage of local faults and fractures. The domes are

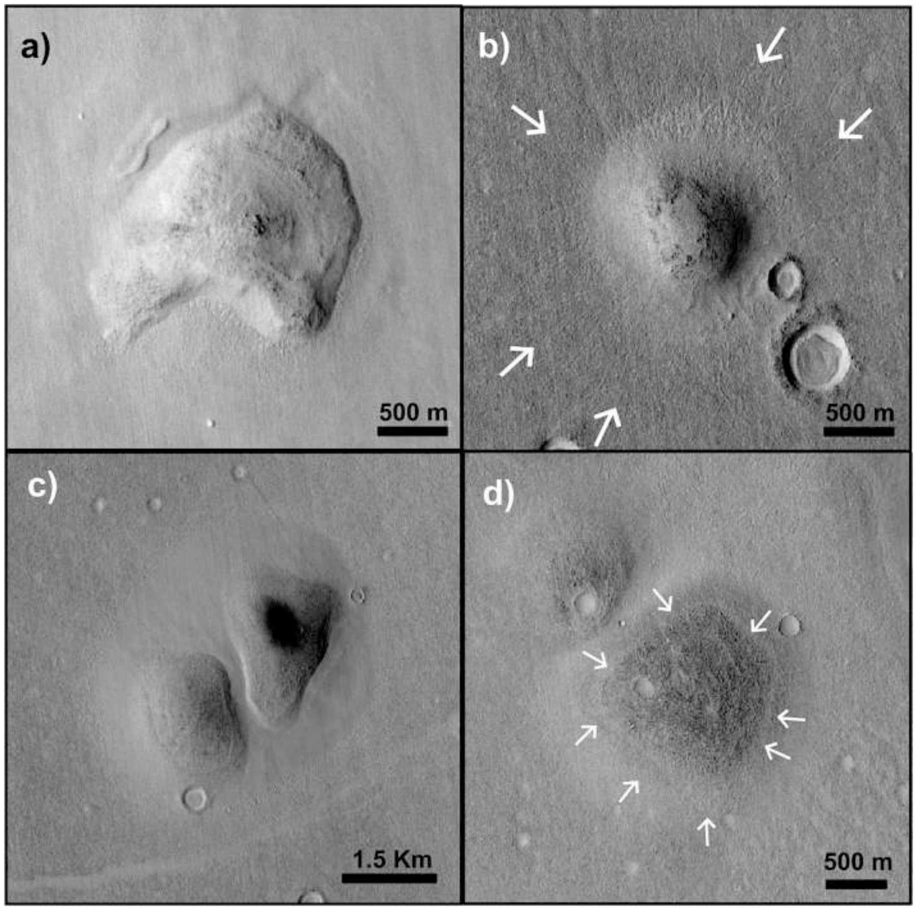

Fig. 16. Different relationships of the aprons with the floor units. The source images are the CTX mosaic. a) Aprons totally covered by the ***Idm*** unit (center coordinates: 38.33°N, 81.53°E). b) Ejecta-like deposits surrounding a subvolcanic uncovered dome (center coordinates: 38.37°N, 79.78°E). c) A pair of domes with well-developed aprons in the ***Fud*** unit (center coordinates: 41.01°N, 79.13°E). d) A pair of domes without aprons, the arrow points to materials of the ***Fud*** unit covering the structure (center coordinates: 38.54°N, 80.29°E).

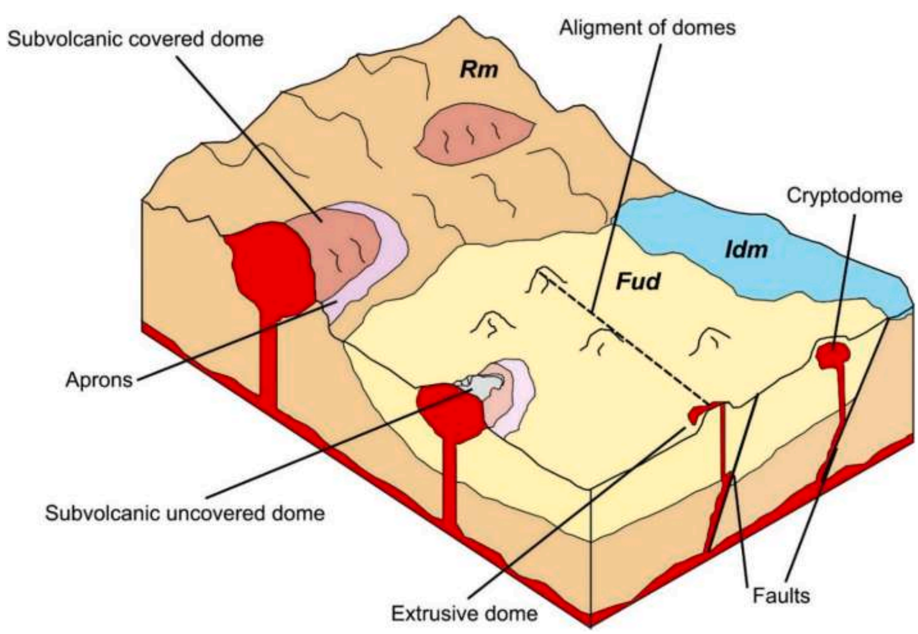

Fig. 17. Sketch representation of the magmatic system under Utopia Planitia and the types of domes that it generated. The upwelling magma likely took advantage of the local fault system to reach the surface.

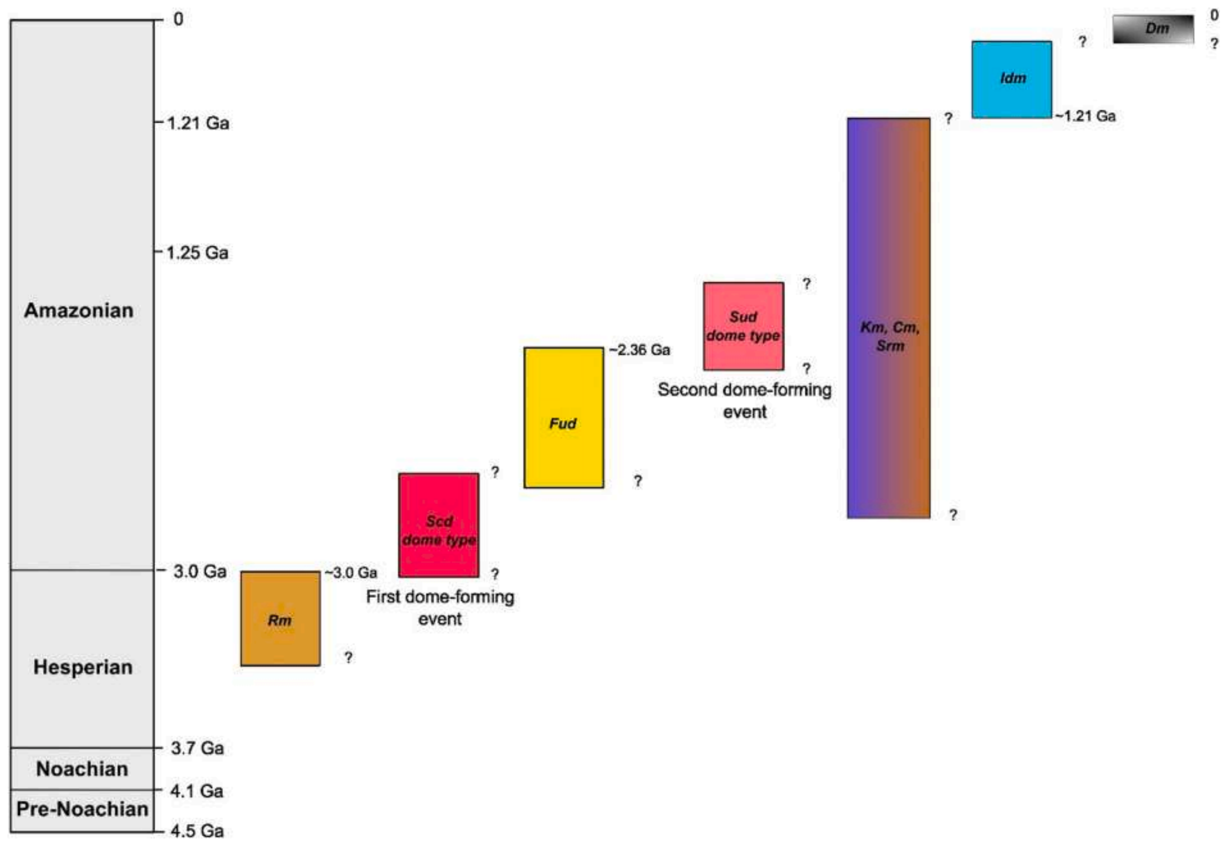

Fig. 18. Geological evolution of the area. Most of the exact ages of the units are unknown, but the sequence of events was defined from stratigraphic relationships.

aligned in a NW-SE trend, which coincides with the trend of the regional faults. Unfortunately, spectral information on the area does not have the best quality, thus, further analysis will be needed to properly assess the composition of the domes and the properties of their parental magmas.

CRediT authorship contribution statement

Javier Eduardo Suárez-Valencia: Writing – original draft, Visualization, Software, Resources, Methodology, Investigation, Formal analysis, Data curation, Conceptualization. **Angelo Pio Rossi:** Writing – review & editing, Validation, Supervision, Resources, Project administration, Investigation, Funding acquisition, Formal analysis, Conceptualization. **Monica Pondrelli:** Writing – review & editing, Visualization, Validation, Supervision, Formal analysis, Conceptualization. **Lucia Marinangeli:** Writing – review & editing, Validation, Supervision, Investigation, Conceptualization. **Vikram Unnithan:** Writing – review & editing, Validation, Supervision, Funding acquisition.

Declaration of competing interest

Hereby I declare for me and my coauthors that we have no conflict of interests in this research.

Acknowledgments

This research was carried out within the framework of the EXPLORE project, which received funding from the European Union's 2020 research and innovation program under grant agreement No 101004214. Additionally, we had support from the GMAP project, part of the Europlanet 2024 RI that has received funding from the European Union's Horizon 2020 research and innovation program under grant agreement No 871149.

Appendix A. Supplementary data

Supplementary data to this article can be found online at https://doi.org/10.1016/j.icarus.2025.116673.

Data availability

The raw datasets used in this work can be accessed through the PDS. The processed geospatial dataset, QGIS project, statistics of the domes, and final maps can also be accessed via Zenodo (Suárez-Valencia et al., 2025).

References

Aileen Yingst, R., Mest, S.C., Brent Garry, W., Williams, D.A., Berman, D.C., Gregg, T.K.P., 2023. A geologic map of Vesta produced using a hybrid method for incorporating spectroscopic and morphologic data. Planet. Sci. J. 4 (9), 157. https://doi.org/10.3847/PSJ/acebe9.

Ballantyne, H.A., Jutzi, M., Golabek, G.J., Mishra, L., Cheng, K.W., Rozel, A.B., Tackley, P.J., 2023. Investigating the feasibility of an impact-induced Martian Dichotomy. Icarus 392, 115395. https://doi.org/10.1016/j.icarus.2022.115395.

Bandfield, J.L., Amador, E.S., 2016. Extensive aqueous deposits at the base of the dichotomy boundary in Nilosyrtis Mensae, Mars. Icarus 275, 29–44. https://doi.org/10.1016/j.icarus.2016.04.002.

Baschetti, B., D'Amore, M., Carli, C., Massironi, M., Altieri, F., 2024, July 3. First Results of Unsupervised Learning Techniques Applied to CRISM Dataset on Mars. https://doi.org/10.5194/epsc2024-756.

Bleacher, J.E., Greeley, R., Williams, D.A., Cave, S.R., Neukum, G., 2007. Trends in effusive style at the Tharsis Montes, Mars, and implications for the development of the Tharsis province. J. Geophys. Res.: Planets 112 (E9), 2006JE002873. https://doi.org/10.1029/2006JE002873.

Bramble, M.S., Mustard, J.F., Salvatore, M.R., 2017. The geological history of Northeast Syrtis Major, Mars. Icarus 293, 66–93. https://doi.org/10.1016/j.icarus.2017.03.030.

Brown, F.F., Pritchard, A.M., 1968. The Mössbauer spectrum of iron orthoclase. Earth Planet. Sci. Lett. 5, 259–260. https://doi.org/10.1016/S0012-821X(68)80049-4.

Brož, P., Bernhardt, H., Conway, S.J., Parekh, R., 2021. An overview of explosive volcanism on Mars. J. Volcanol. Geotherm. Res. 409, 107125. https://doi.org/10.1016/j.jvolgeores.2020.107125.

Burns, R.G., 1993. Mineralogical Applications of Crystal Field Theory, 2.ª ed. Cambridge University Press. https://doi.org/10.1017/CBO9780511524899.
Burr, D.M., Tanaka, K.L., Yoshikawa, K., 2009. Pingos on Earth and Mars. Planet. Space Sci. 57 (5–6), 541–555. https://doi.org/10.1016/j.pss.2008.11.003.
Cañón-Tapia, E., Jacobo-Bojorquez, R.A., 2022. Sub-volcanic structure beneath Marius Hills, moon, inferred from vent distribution. J. Geophys. Res.: Planets 127 (5), e2021JE006960. https://doi.org/10.1029/2021JE006960.
De Pablo, M., Komatsu, G., 2009. Possible pingo fields in the Utopia basin, Mars: geological and climatical implications. Icarus 199 (1), 49–74. https://doi.org/10.1016/j.icarus.2008.09.007.
Dickson, J.L., Ehlmann, B.L., Kerber, L., Fassett, C.I., 2024. The global context camera (CTX) mosaic of Mars: a product of information-preserving image data processing. Earth Space Sci. 11 (7), e2024EA003555. https://doi.org/10.1029/2024EA003555.
Dundas, C.M., McEwen, A.S., 2010. An assessment of evidence for pingos on Mars using HiRISE. Icarus 205 (1), 244–258. https://doi.org/10.1016/j.icarus.2009.02.020.
Edwards, C.S., Nowicki, K.J., Christensen, P.R., Hill, J., Gorelick, N., Murray, K., 2011. Mosaicking of global planetary image datasets: 1. Techniques and data processing for Thermal Emission Imaging System (THEMIS) multi-spectral data. J. Geophys. Res. 116 (E10), E10008. https://doi.org/10.1029/2010JE003755.
Farrand, W.H., Lane, M.D., Edwards, B.R., Aileen Yingst, R., 2011. Spectral evidence of volcanic cryptodomes on the northern plains of Mars. Icarus 211 (1), 139–156. https://doi.org/10.1016/j.icarus.2010.09.006.
Farrand, W.H., Rice, J.W., Chuang, F.C., Rogers, A.D., 2021. Spectral and geological analyses of domes in western Arcadia Planitia, Mars: evidence for intrusive alkali-rich volcanism and ice-associated surface features. Icarus 357, 114111. https://doi.org/10.1016/j.icarus.2020.114111.
Fergason, R.L., Hare, T.M., Laura, J., 2018. HRSC and MOLA Blended Digital Elevation Model at 200m v2. [Dataset]. Astrogeology PDS Annex. https://astrogeology.usgs.gov/search/map/mars_mgs_mola_mex_hrsc_blended_dem_global_200m.
Gillies, S., et al., 2013. Rasterio: Geospatial Raster I/O for Python Programmers. Mapbox. https://github.com/mapbox/rasterio.
Guliyev, I.S., Feizullayev, A.A., Jevanshir, R.D., 1996. All About Mud Volcanoes. Geology Institute, Azerbaijan Academy of Sciences.
Gwinner, K., Jaumann, R., Hauber, E., Hoffmann, H., Heipke, C., Oberst, J., Neukum, G., Ansan, V., Bostelmann, J., Dumke, A., Elgner, S., Erkeling, G., Fueten, F., Hiesinger, H., Hoekzema, N.M., Kersten, E., Loizeau, D., Matz, K.-D., McGuire, P.C., Willner, K., 2016. The High Resolution Stereo Camera (HRSC) of Mars Express and its approach to science analysis and mapping for Mars and its satellites. Planet. Space Sci. 126, 93–138. https://doi.org/10.1016/j.pss.2016.02.014.
Haltigin, T.W., Pollard, W.H., Dutilleul, P., Osinski, G.R., Koponen, L., 2014. Co-evolution of polygonal and scalloped terrains, southwestern Utopia Planitia, Mars. Earth Planet. Sci. Lett. 387, 44–54. https://doi.org/10.1016/j.epsl.2013.11.005.
Harris, C.R., Millman, K.J., Van Der Walt, S.J., Gommers, R., Virtanen, P., Cournapeau, D., Wieser, E., Taylor, J., Berg, S., Smith, N.J., Kern, R., Picus, M., Hoyer, S., Van Kerkwijk, M.H., Brett, M., Haldane, A., Del Río, J.F., Wiebe, M., Peterson, P., Oliphant, T.E., 2020. Array programming with NumPy. Nature 585 (7825), 357–362. https://doi.org/10.1038/s41586-020-2649-2.
Hartmann, W.K., Daubar, I.J., 2017. Martian cratering 11. Utilizing decameter scale crater populations to study Martian history. Meteorit. Planet. Sci. 52 (3), 493–510. https://doi.org/10.1111/maps.12807.
Hauber, E., Brož, P., Jagert, F., Jodłowski, P., Platz, T., 2011. Very recent and wide-spread basaltic volcanism on Mars: recent wide-spread volcanism on Mars. Geophys. Res. Lett. 38 (10), n/a–n/a. https://doi.org/10.1029/2011GL047310.
Hencz, M., Biró, T., Németh, K., Porkoláb, K., Kovács, I.J., Spránitz, T., Cloetingh, S., Szabó, C., Berkesi, M., 2023. Tectonically-determined distribution of monogenetic volcanoes in a compressive tectonic regime: an example from the Pannonian continental back-arc system (Central Europe). J. Volcanol. Geotherm. Res. 444, 107940. https://doi.org/10.1016/j.jvolgeores.2023.107940.
Horgan, B.H.N., Anderson, R.B., Dromart, G., Amador, E.S., Rice, M.S., 2020. The mineral diversity of Jezero crater: evidence for possible lacustrine carbonates on Mars. Icarus 339, 113526. https://doi.org/10.1016/j.icarus.2019.113526.
Hoyer, S., Joseph, H., 2017. xarray: N-D labeled arrays and datasets in Python. J. Open Res. Softw. 5 (1). https://doi.org/10.5334/jors.148.
Hunter, J.D., 2007. Matplotlib: a 2D graphics environment. Comput. Sci. Eng. 9 (3), 90–95. https://doi.org/10.1109/MCSE.2007.55.
Hynek, B.M., Phillips, R.J., Arvidson, R.E., 2003. Explosive volcanism in the Tharsis region: global evidence in the Martian geologic record. J. Geophys. Res.: Planets 108 (E9), 2003JE002062. https://doi.org/10.1029/2003JE002062.
Ivanov, M.A., Hiesinger, H., Erkeling, G., Reiss, D., 2014. Mud volcanism and morphology of impact craters in Utopia Planitia on Mars: evidence for the ancient ocean. Icarus 228, 121–140. https://doi.org/10.1016/j.icarus.2013.09.018.
Jaimes-Viera, M.C., Martin Del Pozzo, A.L., Layer, P.W., Benowitz, J.A., Nieto-Torres, A., 2018. Timing the evolution of a monogenetic volcanic field: Sierra Chichinautzin, Central Mexico. J. Volcanol. Geotherm. Res. 356, 225–242. https://doi.org/10.1016/j.jvolgeores.2018.03.013.
Knapmeyer, M., Oberst, J., Hauber, E., Wählisch, M., Deuchler, C., Wagner, R., 2006. Working models for spatial distribution and level of Mars' seismicity. J. Geophys. Res.: Planets 111 (E11), 2006JE002708. https://doi.org/10.1029/2006JE002708.
Kneissl, T., Van Gasselt, S., Neukum, G., 2011. Map-projection-independent crater size-frequency determination in GIS environments—New software tool for ArcGIS. Planet. Space Sci. 59 (11–12), 1243–1254. https://doi.org/10.1016/j.pss.2010.03.015.
Komatsu, G., Okubo, C.H., Wray, J.J., Ojha, L., Cardinale, M., Murana, A., Orosei, R., Chan, M.A., Ormö, J., Gallagher, R., 2016. Small edifice features in Chryse Planitia, Mars: assessment of a mud volcano hypothesis. Icarus 268, 56–75. https://doi.org/10.1016/j.icarus.2015.12.032.
Laura, J., Acosta, A., Addair, T., Adoram-Kershner, L., Alexander, J., Alexandrov, O., Alley, S., Anderson, D., Anderson, J., Anderson, J., Annex, A., Archinal, B., Austin, C., Backer, J., Barrett, J., Bauck, K., Bauers, J., Becker, K., Becker, T., Young, A., 2023. Integrated Software for Imagers and Spectrometers (Versión 7.2.0_RC1) [Software]. Zenodo. https://doi.org/10.5281/ZENODO.2563341.
Le Corvec, N., Spörli, K.B., Rowland, J., Lindsay, J., 2013. Spatial distribution and alignments of volcanic centers: clues to the formation of monogenetic volcanic fields. Earth Sci. Rev. 124, 96–114. https://doi.org/10.1016/j.earscirev.2013.05.005.
Lefort, A., Russell, P.S., Thomas, N., McEwen, A.S., Dundas, C.M., Kirk, R.L., 2009. Observations of periglacial landforms in Utopia Planitia with the High Resolution Imaging Science Experiment (HiRISE). J. Geophys. Res.: Planets 114 (E4), 2008JE003264. https://doi.org/10.1029/2008JE003264.
Levy, J.S., Head, J.W., Marchant, D.R., 2009. Concentric crater fill in Utopia Planitia: history and interaction between glacial "brain terrain" and periglacial mantle processes. Icarus 202 (2), 462–476. https://doi.org/10.1016/j.icarus.2009.02.018.
Liu, C., Ling, Z., Wu, Z., Zhang, J., Chen, J., Fu, X., Qiao, L., Liu, P., Li, B., Zhang, L., Xin, Y., Shi, E., Cao, H., Tian, S., Wan, S., Bai, H., Liu, J., 2022. Aqueous alteration of the Vastitas Borealis Formation at the Tianwen-1 landing site. Commun. Earth Environ. 3 (1), 280. https://doi.org/10.1038/s43247-022-00614-3.
Malin, M.C., Bell, J.F., Cantor, B.A., Caplinger, M.A., Calvin, W.M., Clancy, R.T., Edgett, K.S., Edwards, L., Haberle, R.M., James, P.B., Lee, S.W., Ravine, M.A., Thomas, P.C., Wolff, M.J., 2007. Context camera investigation on board the Mars Reconnaissance Orbiter. J. Geophys. Res.: Planets 112 (E5), 2006JE002808. https://doi.org/10.1029/2006JE002808.
Mandon, L., Quantin-Nataf, C., Thollot, P., Mangold, N., Lozac'h, L., Dromart, G., Beck, P., Dehouck, E., Breton, S., Millot, C., Volat, M., 2020. Refining the age, emplacement and alteration scenarios of the olivine-rich unit in the Nili Fossae region, Mars. Icarus 336, 113436. https://doi.org/10.1016/j.icarus.2019.113436.
Marinova, M.M., Aharonson, O., Asphaug, E., 2008. Mega-impact formation of the Mars hemispheric dichotomy. Nature 453 (7199), 1216–1219. https://doi.org/10.1038/nature07070.
Mazzarini, F., Isola, I., 2024. The spatial distribution and evolution of volcanic vents in monogenetic fields in active extensional tectonic setting: examples from the northern Main Ethiopian Rift (Ethiopia). J. Volcanol. Geotherm. Res. 451, 108093. https://doi.org/10.1016/j.jvolgeores.2024.108093.
McEwen, A.S., 2007. MRO Mars High Resolution Image Science Experiment EDR V1.0 [Dataset]. NASA Planetary Data System. https://doi.org/10.17189/1520179 (s. f.).
McNeil, J.D., Fawdon, P., Balme, M.R., Coe, A.L., Thomas, N., 2022. Mounds in Oxia Planum: The Burial and Exhumation of the ExoMars Rover Landing Site. J. Geophys. Res. Planets 127 (11), e2022JE007246. https://doi.org/10.1029/2022JE007246.
Michael, G.G., 2013. Planetary surface dating from crater size–frequency distribution measurements: multiple resurfacing episodes and differential isochron fitting. Icarus 226 (1), 885–890. https://doi.org/10.1016/j.icarus.2013.07.004.
Michael, G., 2021. *Craterstats* [Python]. https://github.com/ggmichael/craterstats?tab=BSD-3-Clause-1-ov-file#readme.
Michaut, C., Baratoux, D., Thorey, C., 2013. Magmatic intrusions and deglaciation at mid-latitude in the northern plains of Mars. Icarus 225 (1), 602–613. https://doi.org/10.1016/j.icarus.2013.04.015.
Mills, M.M., McEwen, A.S., Okubo, C.H., 2021. A preliminary regional geomorphologic map in Utopia Planitia of the Tianwen-1 Zhurong Landing Region. Geophys. Res. Lett. 48 (18), e2021GL094629. https://doi.org/10.1029/2021GL094629.
Mouginis-Mark, P., 2018. Olympus Mons volcano, Mars: a photogeologic view and new insights. Geochemistry 78 (4), 397–431. https://doi.org/10.1016/j.chemer.2017.11.006.
Neukum, G., Ivanov, B.A., Hartmann, W.K., 2001. Cratering Records in the Inner Solar System in Relation to the Lunar Reference System. Space Sci. Rev. 96 (1/4), 55–86. https://doi.org/10.1023/A:1011989004263.
Oehler, D.Z., Allen, C.C., 2010. Evidence for pervasive mud volcanism in Acidalia Planitia, Mars. Icarus 208 (2), 636–657. https://doi.org/10.1016/j.icarus.2010.03.031.
Pelkey, S.M., Mustard, J.F., Murchie, S., Clancy, R.T., Wolff, M., Smith, M., Milliken, R., Bibring, J.-P., Gendrin, A., Poulet, F., Langevin, Y., Gondet, B., 2007. CRISM multispectral summary products: parameterizing mineral diversity on Mars from reflectance. J. Geophys. Res.: Planets 112 (E8), 2006JE002831. https://doi.org/10.1029/2006JE002831.
Penasa, L., Brandt, C.H., 2021. europlanet-gmap/mappy: Latest (Versión Latest) [Software]. Zenodo. https://doi.org/10.5281/ZENODO.5233646.
Pieterek, B., Laban, M., Ciążela, J., Muszyński, A., 2022. Explosive volcanism in Noctis Fossae on Mars. Icarus 375, 114851. https://doi.org/10.1016/j.icarus.2021.114851.
Pondrelli, M., Rossi, A.P., Ori, G.G., Van Gasselt, S., Praeg, D., Ceramicola, S., 2011. Mud volcanoes in the geologic record of Mars: the case of Firsoff crater. Earth Planet. Sci. Lett. 304 (3–4), 511–519. https://doi.org/10.1016/j.epsl.2011.02.027.
Quantin-Nataf, C., Lozac'h, L., Thollot, P., Loizeau, D., Bultel, B., Fernando, J., Allemand, P., Dubuffet, F., Poulet, F., Ody, A., Clenet, H., Leyrat, C., Harrisson, S., 2018. MarsSI: Martian surface data processing information system. Planet. Space Sci. 150, 157–170. https://doi.org/10.1016/j.pss.2017.09.014.
Rampey, M.L., Milam, K.A., McSween, H.Y., Moersch, J.E., Christensen, P.R., 2007. Identity and emplacement of domical structures in the western Arcadia Planitia, Mars. J. Geophys. Res.: Planets 112 (E6), 2006JE002750. https://doi.org/10.1029/2006JE002750.
Reiss, D., Fenton, L., Neakrase, L., Zimmerman, M., Statella, T., Whelley, P., Rossi, A.P., Balme, M., 2016. Dust devil tracks. Space Sci. Rev. 203 (1–4), 143–181. https://doi.org/10.1007/s11214-016-0308-6.
Rouault, E., Warmerdam, F., Schwehr, K., Kiselev, A., Butler, H., Łoskot, M., Szekeres, T., Tourigny, E., Landa, M., Miara, I., Elliston, B., Chaitanya, K., Plesea, L.,

Morissette, D., Jolma, A., Dawson, N., 2023. GDAL (Versión v3.7.1) [Software]. Zenodo. https://doi.org/10.5281/ZENODO.5884351.
Schofield, N., Stevenson, C., Mark, N., Holford, S., 2021. Igneous Intrusions: Sills, Dykes and Plutons. In: En *Encyclopedia of Geology*. Elsevier, pp. 313–329. https://doi.org/10.1016/B978-0-08-102908-4.00112-0.
Scholes, D., Guinness, E.A., Slavney, S., Arvidson, R.E., 2021. Introduction to the PDS Geosciences Node Spectral Library Website, 5th Planetary Data and PSIDA 2021, Abstract #7006.
Seelos, F., 2016. MRO Crism Map-Projected Targeted Reduced Data Record V1.0 [dataset]. NASA Planetary Data System. https://doi.org/10.17189/1519470.
Seelos, F.P., Seelos, K.D., Murchie, S.L., Novak, M.A.M., Hash, C.D., Morgan, M.F., Arvidson, R.E., Aiello, J., Bibring, J.-P., Bishop, J.L., Boldt, J.D., Boyd, A.R., Buczkowski, D.L., Chen, P.Y., Clancy, R.T., Ehlmann, B.L., Frizzell, K., Hancock, K. M., Hayes, J.R., Wolff, M.J., 2024. The CRISM investigation in Mars orbit: overview, history, and delivered data products. Icarus 419, 115612. https://doi.org/10.1016/j.icarus.2023.115612.
Smith, I.E.M., Németh, K., 2017. Source to surface model of monogenetic volcanism: a critical review. Geol. Soc. Lond. Spec. Publ. 446 (1), 1–28. https://doi.org/10.1144/SP446.14.
Soare, R.J., Costard, F., Pearce, G.D., Séjourné, A., 2012. A re-interpretation of the recent stratigraphical history of Utopia Planitia, Mars: implications for late-Amazonian periglacial and ice-rich terrain. Planet. Space Sci. 60 (1), 131–139. https://doi.org/10.1016/j.pss.2011.07.007.
Soare, R.J., Conway, S.J., Pearce, G.D., Dohm, J.M., Grindrod, P.M., 2013. Possible crater-based pingos, paleolakes and periglacial landscapes at the high latitudes of Utopia Planitia, Mars. Icarus 225 (2), 971–981. https://doi.org/10.1016/j.icarus.2012.08.041.
Soare, R.J., Horgan, B., Conway, S.J., Souness, C., El-Maarry, M.R., 2015. Volcanic terrain and the possible periglacial formation of "excess ice" at the mid-latitudes of Utopia Planitia, Mars. Earth Planet. Sci. Lett. 423, 182–192. https://doi.org/10.1016/j.epsl.2015.04.033.
Suárez-Valencia, J.E., Rossi, A.P., Pondrelli, M., Marinangeli, L., Unnithan, V., 2025. Supporting Material for: Geological Analysis of the Dome Field in Western Utopia Planitia, on Mars [Data Set]. Zenodo. https://doi.org/10.5281/zenodo.15168483.
Sunshine, J.M., Pieters, C.M., 1998. Determining the composition of olivine from reflectance spectroscopy. J. Geophys. Res.: Planets 103 (E6), 13675–13688. https://doi.org/10.1029/98JE01217.
Tanaka, K.L., Skinner, J.A., Hare, T., 2005. *Geologic Map of the Northern Plains of Mars* [Map].
Tanaka, K.L., Skinner, J.A., Dohm, J.M., Irwin, R.P., Kolb, E.J., Fortezzo, C.M., Platz, T., Michael, G.G., Hare, T.M., 2014. *Geologic map of Mars (pamphlet 43 p.) [Map]*.
Trippanera, D., Ruch, J., Acocella, V., Thordarson, T., Urbani, S., 2018. Interaction between central volcanoes and regional tectonics along divergent plate boundaries: Askja, Iceland. Bull. Volcanol. 80 (1), 1. https://doi.org/10.1007/s00445-017-1179-8.
Viviano, C.E., Seelos, F.P., Murchie, S.L., Kahn, E.G., Seelos, K.D., Taylor, H.W., Taylor, K., Ehlmann, B.L., Wiseman, S.M., Mustard, J.F., Morgan, M.F., 2014. Revised CRISM spectral parameters and summary products based on the currently detected mineral diversity on Mars. J. Geophys. Res.: Planets 119 (6), 1403–1431. https://doi.org/10.1002/2014JE004627.
Werner, S.C., 2009. The global martian volcanic evolutionary history. Icarus 201 (1), 44–68. https://doi.org/10.1016/j.icarus.2008.12.019.
Wieczorek, M.A., Broquet, A., McLennan, S.M., Rivoldini, A., Golombek, M., Antonangeli, D., Beghein, C., Giardini, D., Gudkova, T., Gyalay, S., Johnson, C.L., Joshi, R., Kim, D., King, S.D., Knapmeyer-Endrun, B., Lognonné, P., Michaut, C., Mittelholz, A., Nimmo, F., Banerdt, W.B., 2022. InSight constraints on the global character of the Martian Crust. J. Geophys. Res.: Planets 127 (5), e2022JE007298. https://doi.org/10.1029/2022JE007298.
Williams, J., Nimmo, F., Moore, W.B., Paige, D.A., 2008. The formation of Tharsis on Mars: what the line-of-sight gravity is telling us. J. Geophys. Res.: Planets 113 (E10), 2007JE003050. https://doi.org/10.1029/2007JE003050.
Wright, J., Zambon, F., Carli, C., Altieri, F., Pöhler, C.M., Rothery, D.A., Van Der Bogert, C.H., Rossi, A.P., Massironi, M., Balme, M.R., Conway, S.J., 2024. A geostratigraphic map of the Rachmaninoff Basin Area: integrating morphostratigraphic and spectral units on Mercury. Earth Space Sci. 11 (2), e2023EA003258. https://doi.org/10.1029/2023EA003258.
Zhang, T., Wang, L., Saidamat, A., Xiao, L., Huang, J., 2023. Evolution history of mesas in the Southern Utopia Planitia and implications for the ancient oceans on Mars. J. Earth Sci. 34 (3), 940–950. https://doi.org/10.1007/s12583-022-1776-0.